

Fast rotating massive stars and the origin of the abundance patterns in galactic globular clusters

T. Decressin¹, G. Meynet¹, C. Charbonnel^{1,2}, N. Prantzos³, and S. Ekström¹

¹ Geneva Observatory, University of Geneva, chemin des Maillettes 51, 1290 Sauverny, Switzerland

² Laboratoire d'Astrophysique de Toulouse et Tarbes, CNRS UMR 5572, OMP, 14, Av. E.Belin, 31400 Toulouse, France

³ Institut d'Astrophysique de Paris, CNRS UMR 7095, Univ. P. & M.Curie, 98bis Bd. Arago, 75104 Paris, France

Received / Accepted

ABSTRACT

Aims. We propose the Wind of Fast Rotating Massive Stars scenario to explain the origin of the abundance anomalies observed in globular clusters.

Methods. We compute and present models of fast rotating stars with initial masses between 20 and 120 M_{\odot} for an initial metallicity $Z=0.0005$ ($[Fe/H] \approx -1.5$). We discuss the nucleosynthesis in the H-burning core of these objects and present the chemical composition of their ejecta. We consider the impact of uncertainties in the relevant nuclear reaction rates.

Results. Fast rotating stars reach the critical velocity at the beginning of their evolution and remain near the critical limit during the rest of the main sequence and part of the He-burning phase. As a consequence they lose large amounts of material through a mechanical wind which probably leads to the formation of a slow outflowing disk. The material in this slow wind is enriched in H-burning products and presents abundance patterns similar to the chemical anomalies observed in globular cluster stars. In particular, the C, N, O, Na and Li variations are well reproduced by our model. However the rate of the $^{24}Mg(p, \gamma)$ has to be increased by a factor 1000 around 50×10^6 K in order to reproduce the whole amplitude of the observed Mg-Al anticorrelation. We discuss how the long-lived low-mass stars currently observed in globular clusters could have formed out of the slow wind material ejected by massive stars.

Key words. Nuclear reactions, nucleosynthesis, abundances - Stars: rotation - Stars: mass-loss - Stars: abundances - globular clusters: general - globular clusters: individual: NGC 6752

1. Introduction

Galactic globular clusters (hereafter GCs) appear to be chemically homogeneous (with the notable exception of ω Cen) with respect to the iron-group (Mn, Fe, Ni, Cu), neutron-capture (Ba, La, Eu) and alpha-elements (Si, Ca) (e.g., Kraft et al. 1992; James et al. 2004a,b; Sneden 2005; Sobeck et al. 2006). However it has long been known that these large aggregates of stars show strong inhomogeneities in lighter elements: C, N, O, Na, Mg and Al abundances present indeed large star-to-star abundance variations within all the individual GCs studied up to now (for complete references see the early reviews by Freeman & Norris 1981, Smith 1987, and Kraft 1994 and the more recent ones by Gratton et al. 2004 and Charbonnel 2005).

The observed patterns point to the simultaneous operation of the CNO, NeNa and MgAl cycles of hydrogen-burning: C and N, O and Na, and Mg and Al are respectively anticorrelated, the abundances of C, O and Mg being depleted while those of N, Na and Al are enhanced. Whenever C, N, and O are observed simultaneously, their sum appears to be constant within the observational errors (e.g., Dickens et al. 1991; Ivans et al. 1999). The sum Mg+Al is also found to be constant in several clusters (Shetrone 1996). Observations in NGC 6752, M 13 and M 71 show that the Mg depletion is due to the burning of ^{24}Mg while ^{25}Mg is untouched and ^{26}Mg is produced in the Al-rich stars (Yong et al. 2003, 2005, 2006). Last but not least, Li was

found to be anticorrelated with Na in turn-off stars of NGC 6752 (Pasquini et al. 2005). All these features are considered anomalous because they are not seen in field stars of similar metallicity (e.g., Gratton et al. 2000).

For many years only the brightest GC red giants were accessible for detailed spectroscopic observations, and two main theoretical streams were competing to explain the available data: (1) the so-called “evolution” scenario according to which the chemical anomalies are generated inside the low-mass stars we are presently observing, and (2) the “self-enrichment” (or primordial) scenario according to which such patterns pre-existed in the protocluster gas and were inherited at the birth of the long-lived stars.

The evolution hypothesis has been seriously challenged by recent spectroscopic observations of less luminous stars in earlier stages of evolution in a number of GCs. Such studies revealed indeed that stars located slightly above and below the main sequence turnoff exhibit the same anomalies as their giant counterparts (Gratton et al. 2001; Grundahl et al. 2002; Carretta et al. 2003, 2004; Cohen et al. 2002; Ramírez & Cohen 2002, 2003; Harbeck et al. 2003). However such objects are not hot enough¹ for the required set of nuclear reactions to occur within their interior. Let us recall that while the CNO cycle is activated for temperatures above 20×10^6 K, the NeNa and MgAl chains require temperatures around 35×10^6 K and 50×10^6 K respectively. Destruction of ^{24}Mg by proton-capture needs still

Send offprint requests to: T. Decressin,
e-mail: Thibaut.Decressin@obs.unige.ch

¹ In the central region of a $0.85 M_{\odot}$, $[Fe/H] = -1.3$ turnoff star, the temperature is of the order of 25×10^6 K.

higher temperatures, around 70×10^6 K (e.g., Arnould et al. 1999; Prantzos & Charbonnel in preparation). As a consequence the abundance variations cannot be produced in situ, but certainly reflect the initial composition of the protostars. It is thus clear now that a large fraction of GC low-mass stars were formed from material processed through H-burning at high temperatures and then lost by more massive and faster evolving stars, and perhaps mixed with some original gas. Various aspects of this “self-enrichment scenario” are discussed in details by Prantzos & Charbonnel (2006, hereafter PC06).

Regarding the nucleosynthetic site, most studies have focused on massive AGB stars which were suggested as the possible polluters by Cottrell & Da Costa (1981). The two main reasons why these objects have been favored are that (1) they host regions where H-burning occurs at high temperatures (in particular when they experience the so-called hot bottom burning, or HBB, at the base of their convective envelope between successive thermal pulses), and (2) the material they eventually eject (by stellar winds or Roche lobe overflow) is not enriched in iron. This last property is well consistent with the observational fact recalled above that the iron abundance in a GC does not show any significant scatter. For long the AGB hypothesis was discussed only on a qualitative basis. However recent custom-made stellar models (Ventura et al. 2001, 2002; Denissenkov & Herwig 2003; Karakas & Lattanzio 2003; Herwig 2004a,b; Ventura & D’Antona 2005a,b,c, 2006; Decressin et al., in preparation) pointed out very severe difficulties from the nucleosynthesis point of view which stem from the competition between the HBB and the third dredge-up. This latest process does indeed contaminate the envelope of the AGB with the products of helium burning and creates abundance patterns in conflict with the observed ones (see Fenner et al. 2004 and Charbonnel 2005 for more details). PC06 discuss other shortcomings of the AGB scenario, the main one being related to the peculiar initial mass function it requires. In addition, they underline the fact that the AGB scenario gives no satisfactory answer as to the role of stars more massive and less massive than the presumed polluters.

Massive stars, more precisely, Wolf-Rayet stars, have been proposed by Brown & Wallerstein (1993) and by Wallerstein et al. (1987) as possible sources for the very early enrichment of globular clusters. More recently Maeder & Meynet (2006) suggested that He-rich stars in ω Cen could be formed from wind material of fast rotating massive stars. Prantzos & Charbonnel (2006) proposed a comprehensive (albeit qualitative) scenario for the role of massive stars, suggesting that their winds provide the metal-enriched material for the next stellar generation, and that the subsequent supernova explosions provide the trigger for the star formation; the SN ejecta escape altogether the GC environment, along the cavities opened previously by the stellar winds. PC06 also studied the massive star IMF required to explain quantitatively the amount of Na-enhanced stars observed in NGC 2708 and found it to be flatter than canonical (i.e. Salpeter) IMFs; even flatter IMFs would be required in case the polluters were AGB stars. Similar conclusions for a flat IMF are reached by Smith (2006), for the case of N enhancement of GC by massive star winds. The main reason why such objects have been discarded in the past in the context of the self-enrichment scenario is related to the fact that iron is ejected at the time of their supernova explosion and this constitutes a priori a serious drawback for considering massive stars as GC pollution sources. This is true unless some filtering process removes the ejecta enriched by helium burning and more advanced nuclear stages while

preserving those bearing the signatures of hydrogen processing. This is the key point of the *Winds of Fast Rotating Massive Stars* scenario (hereafter WFRMS) that we propose in the present work. In our framework, the GC chemical anomalies are built in H-burning zones of massive stars. Rotational mixing brings to the surface CNO-processed material which can then be ejected in a slow wind when the stars rotate at the critical limit.

As shown by Sackmann & Anand (1970) and later by Langer (1998) and Maeder & Meynet (2001), massive stars do reach the so-called critical velocity² early on the main sequence if (1) they start their evolution with a sufficiently high initial rotation rate, (2) they do not lose too much angular momentum through stellar winds and (3) an efficient mechanism (meridional circulation in our models) transports angular momentum from the core to the envelope. Once the critical limit is reached, the surface velocity remains near the critical value during the rest of the main sequence and very likely an equatorial disk is formed as observed for instance around Be stars. In the case of these stars, only minor outflow in the line-forming region is observed (see the review by Porter & Rivinius 2003). This material has thus a great chance to be retained in the GC potential well. On the other hand fast rotation leads to strong internal mixing of the chemicals. As a result the ejected material will present the marks of H-processing occurring in the stellar core. Thus if new stars form out of the slow wind material, their composition would bear the signatures of H-burning. The main question addressed in this paper is whether the chemical composition of the ejecta of fast rotating massive stars is compatible with what observed in the long-lived GC stars.

In the present paper we develop in details the WFRMS scenario. In § 2 we describe the physical ingredients of our models of rotating massive stars. We first focus on the properties of the $60 M_{\odot}$ models computed with various assumptions. For this initial stellar mass we discuss the nucleosynthesis in the H-burning core in § 3 while in § 4 we investigate the chemical composition of the wind ejecta. The full range of masses between 20 and $120 M_{\odot}$ is investigated in § 5. In § 6 comparisons between the wind composition and the GC abundance patterns are performed. A schematic and speculative discussion of the complete scenario for explaining the inhomogeneities in GCs is presented in § 7. The conclusions and some future lines of research are given in § 8.

2. Physical inputs

Our stellar models were computed with the Geneva evolution code including the effects of rotation (Meynet & Maeder 2000). We focus on the mass range corresponding to stars with high enough central temperatures on the main sequence for the NeNa and MgAl chains (see Fig. 1) to be activated. Models with initial masses of 20, 40, 60, and $120 M_{\odot}$ are computed from the Zero Age Main Sequence up to the end of the core He-burning phase, and a $200 M_{\odot}$ model is computed up to the end of the core H-burning phase. The theoretical predictions for the $60 M_{\odot}$ star are discussed in detail in § 3 and 4 in order to properly illustrate the WFRMS scenario.

2.1. Microphysics

We use the OPAL opacities (Iglesias & Rogers 1996), complemented at temperatures below 5000 K with the

² By critical velocity, we mean the equatorial surface velocity such that the centrifugal acceleration exactly balances the gravity.

molecular opacities of Alexander & Ferguson (1994) (<http://webs.wichita.edu/physics/opacity>).

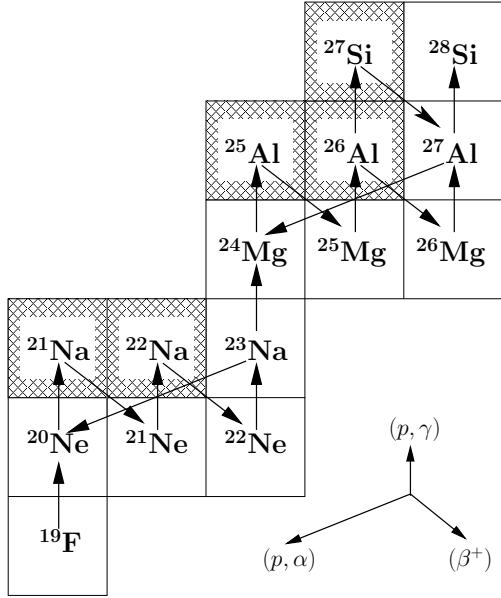


Fig. 1. Network of nuclear reactions involved in the NeNa and MgAl chains. Unstable nuclei are in shaded boxes. Arrows indicate the type of nuclear reactions: (p, γ) , β^+ , and (p, α)

Table 1. Main physical inputs of the stellar models for the various initial masses considered. The labels “r” and “s” indicate respectively the models computed with or without rotation while the labels A-D refer to the choices in nuclear reactions (see text and Table 2). The initial value of $\Omega/\Omega_{\text{crit}}$ is given. [I], [H02] and [H04] correspond respectively to Iliadis et al. (2001) and Hale et al. (2002, 2004)

M (M_{\odot})	Label	$\Omega/\Omega_{\text{crit}}$	Nuclear rates
60	60rA	0.95	set A [†] : NACRE (nominal)
	60rB	0.95	set B [†] : [I, H02, H04] (nominal)
	60rC	0.95	set C [†] : [I, H02, H04] (exp. limits)
	60rD	0.95	set D [†]
	60rE	0.80	set C
20	20rC	0.95	set C
40	40rC	0.98	set C
120	120rC	0.80	set C
200	200rC	0.95	set C
20	20sC	0	set C
40	40sC	0	set C
60	40sC	0	set C
120	120sC	0	set C

[†] Details on the nuclear rates used are presented in Table 2.

In order to investigate the effects of the nuclear reaction rate uncertainties on the products of hydrogen nucleosynthesis, we present four models for the 60 M_{\odot} star computed using different sets of nuclear reactions for the hydrogen-burning network (see Table 1). Set A uses all the nominal values of the NACRE compilation (Angulo et al. 1999). The three other cases include the updates of Iliadis et al. (2001) and Hale et al. (2002, 2004) for the reactions involved in the NeNa and MgAl chains but with different options (see Table 2). Set B includes nominal values

Table 2. Nuclear reaction rates adopted for the NeNa- and MgAl-chains in the sets B-D. [N], [I], [H02] and [H04] correspond respectively to Angulo et al. (1999), Iliadis et al. (2001) and Hale et al. (2002, 2004). “Nom.,” “low.” and “up.” refer respectively to nominal, lower and upper limits of the experimental values. For all the other reactions of our network we use the NACRE nominal values

Reaction	set A	set B	set C	set D
$^{20}\text{Ne}(p, \gamma)$	[N], nom.	[N], nom.	[N], low.	[N], low.
$^{21}\text{Ne}(p, \gamma)$	[N], nom.	[I], nom.	[I], low.	[I], low.
$^{22}\text{Ne}(p, \gamma)$	[N], nom.	[H2], nom.	[H2], low.	[H2], low.
$^{23}\text{Na}(p, \gamma)$	[N], nom.	[H4], nom.	[H4], low.	[H4], low.
$^{23}\text{Na}(p, \alpha)$	[N], nom.	[H4], nom.	[H4], up.	[H4], up.
$^{24}\text{Mg}(p, \gamma)$	[N], nom.	[I], nom.	[I], up.	[I], +3 dex
$^{25}\text{Mg}(p, \gamma)$	[N], nom.	[I], nom.	[I], up.	[I], up.
$^{26}\text{Mg}(p, \gamma)$	[N], nom.	[I], nom.	[I], up.	[I], up.
$^{27}\text{Al}(p, \gamma)$	[N], nom.	[I], nom.	[I], low.	[I], low.
$^{27}\text{Al}(p, \alpha)$	[N], nom.	[I], nom.	[I], low.	[I], low.

while in set C some specific rates are set to the experimental upper or lower limits. Fig. 2 presents the corresponding rates for the temperature range between 30×10^6 and 80×10^6 K which is typical of the central temperatures of our main sequence stars. Finally set D is similar to set C except for the proton-capture on ^{24}Mg which is increased by three orders of magnitude compared to Iliadis et al. (2001) nominal value around 50×10^6 K.

The initial composition of the chemical mixture is given in Table 3. It corresponds to that used to compute the opacity tables (Iglesias & Rogers 1996, Weiss alpha-enhanced elements mixture). The metallicity of our models is $[\text{Fe}/\text{H}] \simeq -1.5$ corresponding to that of NGC 6752 which is the GC with the largest set of abundance data. The initial isotopic ratios of magnesium are taken equal to 80:10:10; this corresponds to the values observed in NGC 6752 “unpolluted” stars (i.e., in stars with high O and low Na abundances) in contrast with “polluted” stars which display large O depletion with high Na abundance (Yong et al. 2003, 2006).

Table 3. Initial abundances in mass fraction

Element	Abundance	Element	Abundance
^1H	0.754	^{19}F	1.53e-8
^3He	2.93e-5	^{20}Ne	5.30e-5
^4He	0.245	^{21}Ne	5.00e-8
^{12}C	3.50e-5	^{22}Ne	4.72e-6
^{13}C	1.47e-7	^{23}Na	3.30e-7
^{14}N	1.03e-5	^{24}Mg	1.68e-5
^{15}N	1.58e-8	^{25}Mg	2.10e-6
^{16}O	3.00e-4	^{26}Mg	2.10e-6
^{17}O	1.31e-7	^{27}Al	9.00e-7
^{18}O	7.45e-6	^{28}Si	2.56e-5

2.2. Rotation and mass loss

We follow the formalism by Zahn (1992) and Maeder & Zahn (1998) for the transport of angular momentum and chemicals in rotating stars. The effects of both meridional circulation and shear turbulence are taken into account: the meridional circulation advects angular momentum and the shear acts as a diffusive process. The transport of chemical species is computed as a diffusive process as the result of meridional circulation and

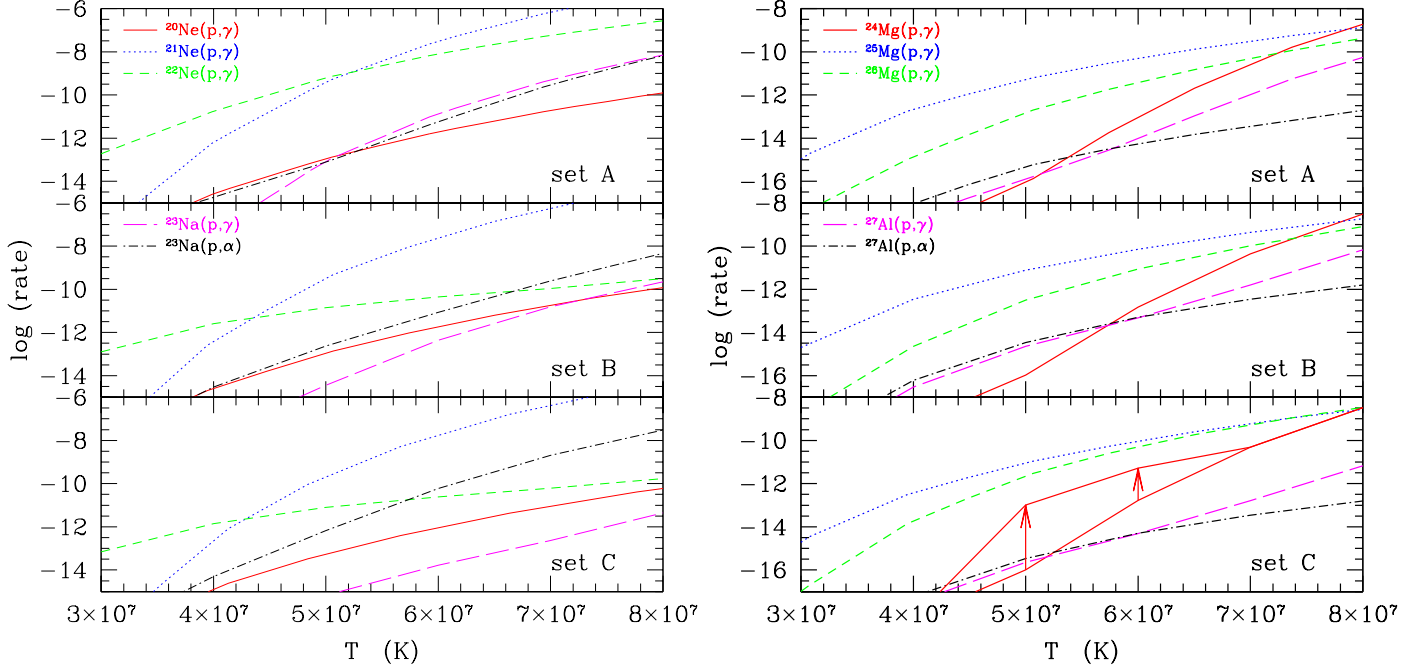


Fig. 2. Nuclear reaction rates for NeNa (left) and MgAl chains (right) from the set A, B and C (top to bottom). Arrows and upper full line in the lower right panel indicate the increase of the rate of $^{24}\text{Mg}(p,\gamma)^{25}\text{Al}$ at $T = 50$ and 60×10^6 K assumed in set D.

horizontal and vertical turbulence (Chaboyer & Zahn 1992). The treatment of the convective instability is done according to the Schwarzschild criterion and we do not consider overshooting.

The treatment of rotation includes the hydrostatic effects following Meynet & Maeder (1997) as well as the impact of rotation on the mass loss rate described by Maeder & Meynet (2000). We do not account for the wind anisotropies induced by rotation as in Maeder (1999) although the related effects would reinforce the trends found in this paper by fastening the arrival at the break-up limit (see § 4.1).

The radiative mass loss rates are from Kudritzki & Puls (2000) when $\log T_{\text{eff}} > 3.95$ and from de Jager et al. (1988) otherwise. When a model reaches the WR phase (i.e., when the surface hydrogen mass fraction becomes lower than 0.4 and the effective temperature is higher than 10^4 K), the mass loss rate is switched to the prescription of Nugis & Lamers (2000). Except for the WR phase, we consider a dependence of the mass loss rates with metallicity as $\dot{M} \propto \sqrt{Z/Z_{\odot}}$, where Z is the mass fraction of heavy elements at the surface of the star.

As in Meynet et al. (2006) a specific treatment for mass loss has been applied at break-up. Let us recall that according to Meynet & Maeder (2000) three kinds of “break-up limits” can be defined depending on which mechanism (i.e., radiative acceleration, centrifugal acceleration or both) contributes to counterbalance the gravity: 1.– The Γ -Limit, when radiation effects largely dominate; 2.– The Ω -Limit, when rotation effects are essentially determining break-up; 3.– The $\Omega\Gamma$ -Limit, when both rotation and radiation are important for the critical velocity. In the present work the Ω -Limit is reached during the MS, while the $\Omega\Gamma$ -Limit is encountered by our most massive stellar models ($M \geq 60 M_{\odot}$) just after the MS.

During the MS, near the Ω -Limit, two counteracting effects are competing. On one hand, matter is removed from the stellar surface (mainly through the equatorial regions) together with angular momentum. Also the expansion of the envelope tends to slow down the surface. On the other hand, meridional advection

in the outer layers acts so as to transfer angular momentum from the inner stellar regions to the surface (see for instance Fig. 1 in Meynet & Maeder 2002). This acts as to accelerate the surface. As long as the internal transport of angular momentum is efficient enough for accelerating the outer layers in a timescale shorter than the mass loss or inflation timescale, the surface velocity remains near the critical limit. In practice, however, the critical limit contains mathematical singularities; we thus consider that during the break-up phase, the mass loss rate is such that the rotation velocity stays near a constant fraction of the critical value (0.98 typically). At the end of the main sequence, the stellar radius inflates so rapidly that meridional circulation cannot anymore ensure the internal coupling and the break-up phase ceases naturally. However the most massive stellar models encounter the $\Omega\Gamma$ -Limit after the MS. In that case, we apply similar procedures as the one described above, i.e. we apply mass loss rates that maintain the model at a constant distance from the $\Omega\Gamma$ -Limit. When the star has lost sufficient amount of mass for evolving away from this limit, the regular mass loss rates apply again.

For the reasons invoked in the introduction and which will be discussed again later, we explore the case of high initial rotational velocities. For the stars with initial mass between 40 and $120 M_{\odot}$ we take $V_{\text{ini}} = 800 \text{ km s}^{-1}$. The $200 M_{\odot}$ model starts with $V_{\text{ini}} = 1000 \text{ km s}^{-1}$. This corresponds to an initial value of $\Omega/\Omega_{\text{crit}}$ between 0.80 and 0.98. The $20 M_{\odot}$ star starts with $V_{\text{ini}} = 600 \text{ km s}^{-1}$ as it nearly corresponds to the break-up velocity ($\Omega/\Omega_{\text{crit}} = 0.95$).

3. Central hydrogen-burning in a $60 M_{\odot}$ star

As a prerequisite to our scenario we first have to check whether the abundance patterns due to nuclear reactions in the hydrogen-burning core of massive stars do mimic the chemical trends observed in GC low-mass stars. Obviously the abundance variations obtained within the central regions are the most extreme

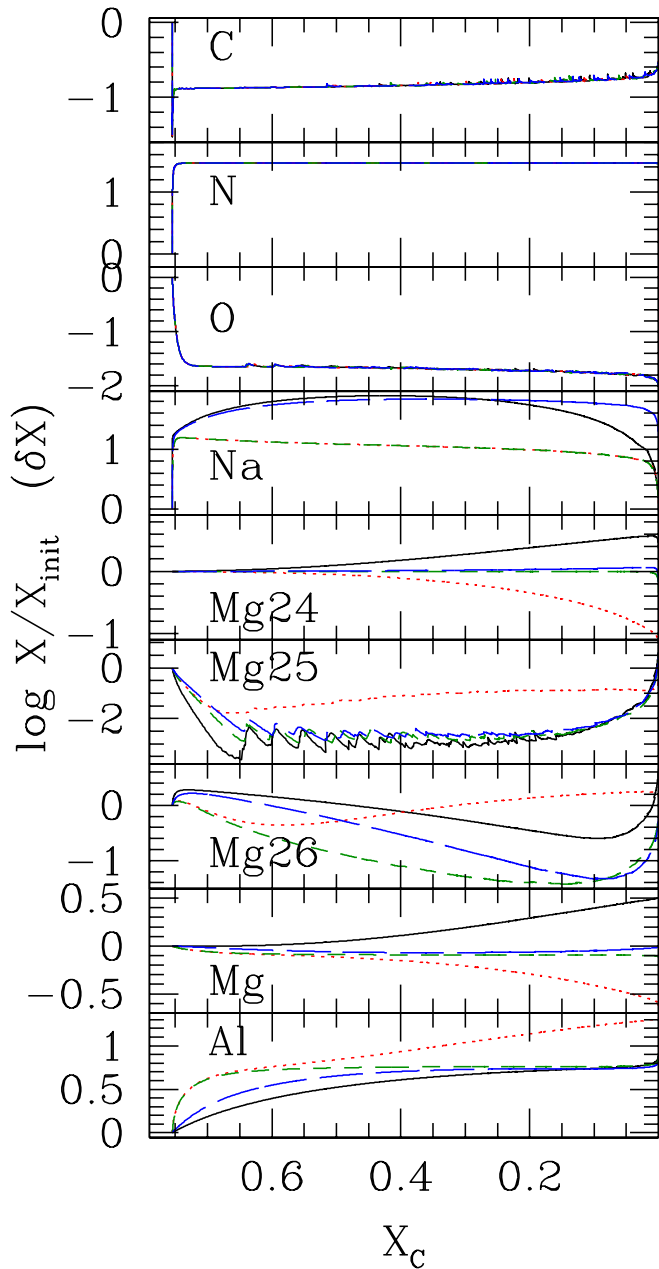


Fig. 3. Evolution of the central abundances in the $60 M_{\odot}$ rotating models computed with different sets of nuclear reaction rates: set A (full line), set B (long dashed lines), set C (short dashed lines) and set D (dotted lines). The amount of the unstable nucleus ^{26}Al is added to those of ^{26}Mg and Mg.

ones that one can expect within the WFRMS scenario. Indeed some dilution of this processed material is expected in the radiative envelope of the polluters (see § 4) and then eventually later with the intracluster gas (see § 6). We are thus looking for stronger abundance variations in the stellar core than the presently observed ones for the elements involved in the CNO, NeNa and MgAl cycles.

We first investigate the nucleosynthesis that occurs within the convective core of a main sequence $60 M_{\odot}$ star and we explore in detail the uncertainties of the nuclear reaction rates. The evolution of the central abundances of the key elements is pre-

sented in Fig. 3 as a function of the central abundance of hydrogen for the various sets of nuclear reactions (see Table 2).

3.1. CNO nucleosynthesis

In the $60 M_{\odot}$ star the central temperature on the main sequence varies from 48×10^6 K to 75×10^6 K (see Fig. 7). The CNO cycle thus rapidly reaches equilibrium at the beginning of H-burning. As a result the central abundance of ^{12}C drops suddenly by about an order of magnitude, while that of ^{14}N increases by a factor of 29. Slightly later ^{16}O does reach its equilibrium value, which is 1.6 dex below its initial abundance. After this adjustment phase at the very beginning of the main sequence, the CNO elements stay at their equilibrium level. These predictions are identical for all the $60 M_{\odot}$ models presented here because they were all computed with NACRE prescriptions for the CNO-cycle reaction rates (no modification of these rates has been published since the NACRE compilation was made available).

3.2. NeNa and MgAl predictions with the NACRE nominal values - Model 60rA

Model 60rA was computed with the NACRE nominal values for the whole nuclear network (full lines on Fig. 3).

As can be seen on Fig. 3, the central abundance of ^{23}Na shows a three steps evolution on the main sequence: a first rapid raise by 1.2 dex, then a more progressive increase of 0.7 dex until the mass fraction of hydrogen at the center, X_c , equals 0.4, and finally a decrease. The initial feature is due to proton-captures on ^{21}Ne and ^{22}Ne which are the fastest reactions of the NeNa chain (see Fig. 2). As proton-capture on ^{23}Na is slower, the abundance of sodium increases until the complete consumption of ^{21}Ne and ^{22}Ne . Later on ^{20}Ne starts burning in favor of sodium. The slow increase is due to the competition between the burning of ^{20}Ne and that of ^{23}Na via the channels (p, γ) or (p, α) . When using NACRE nominal values the transformation of ^{20}Ne into ^{23}Na is more efficient than the ^{23}Na destruction for T inferior to $\sim 50 \times 10^6$ K which results in a slow increase of ^{23}Na . When the temperature exceeds 50×10^6 K the situation reverses and the abundance of ^{23}Na decreases.

Let us now turn our attention to Mg and Al. In model 60rA the central abundance of ^{24}Mg increases slightly during the main sequence. That of ^{25}Mg first decreases by nearly 4 dex, then it presents a sawtooth behavior until X_c equals ~ 0.2 and finally it increases. ^{26}Mg first slightly increases before decreasing during most of the core H-burning phase and increasing again when X_c becomes lower than ~ 0.07 . The behavior of Mg (total) follows mainly that of ^{24}Mg . Last but not least, the abundance of Al increases.

The increase of the ^{24}Mg abundance is due to proton-captures on ^{23}Na . The very efficient destruction of ^{25}Mg is due to the reaction $^{25}\text{Mg}(p, \gamma)^{26}\text{Al}$. The sawtooth behavior results from small instabilities affecting the size of the convective core.³ The slight production of this element at the end of the main sequence is due to the proton-captures on ^{24}Mg . The initial raise of the abundance of ^{26}Mg results from the destruction of ^{25}Mg de-

³ When the size of the convective core slightly increases, some ^{25}Mg is dredged down. For most elements, the quantity dredged down is small compared to the abundance in the core; however in the case of ^{25}Mg which is severely depleted in the core, this temporarily produces a small increase of the central abundance.

scribed above.⁴ When all the ^{25}Mg is consumed within the core, ^{26}Mg is converted into aluminum.

Table 4 sums-up the mean variations of the central abundances during the main sequence for the NACRE nominal reaction rates. O and Na are respectively depleted and produced as required by the data. On the other hand the increase of the total magnesium we obtain is at odds with the observed Mg-Al anticorrelation. These results agree with those of Arnould et al. (1999) who investigated in details hydrogen-nucleosynthesis at constant temperature and solar metallicity with NACRE reaction rates. They found a production of Na and they argue that it is dominated by uncertainties on the rates for $T > 50 \times 10^6$ K. Also ^{24}Mg is not destroyed even when experimental errors on rates are taken into account for $T < 70 \times 10^6$ K. Production of aluminum is due to the burning of both ^{25}Mg and ^{26}Mg .

3.3. NeNa and MgAl predictions with the Iliadis nominal values - Model 60rB

In model 60rB we take into account the nominal rates given by Iliadis et al. (2001) and Hale et al. (2002, 2004) for the reactions involved in the NeNa and MgAl chains. The differences with the NACRE prescriptions can be seen in Fig. 2. At $T = 50 \times 10^6$ K the rates of the $^{22}\text{Ne}(p, \gamma)$ and $^{23}\text{Na}(p, \gamma)$ reactions are lowered respectively by 1.7 dex and 1.3 dex compared to NACRE nominal values, while the rate of $^{23}\text{Na}(p, \alpha)$ is 0.6 dex higher. For $^{27}\text{Al}(p, \gamma)$ the new rate is increased by 1 dex at $T = 50 \times 10^6$ K, but is unchanged for $T > 70 \times 10^6$ K. Finally the rate of the $^{27}\text{Al}(p, \alpha)^{24}\text{Mg}$ reaction is now higher by 0.7 to 1.1 dex in the range of temperature of interest. The prescriptions for the other reactions are unchanged.

This update does not affect the global structure and evolution of the star, as the energizing rates concern the CNO cycle which is not modified. Thus the lifetime, the size of the convective core as well as the mass loss history are identical in all our models.

The key reaction for the NeNa chain is $^{20}\text{Ne}(p, \gamma)$ as ^{20}Ne is the most abundant neon isotope and its destruction by proton-captures is much slower than that of the ^{21}Ne and ^{22}Ne (by 2.7 and 3.7 orders of magnitude respectively). Since the rate of this reaction is unchanged the behavior of the Ne isotopes is barely affected with respect to the results presented in § 3.2. On the other hand because the rate of proton-capture on ^{23}Na is reduced now with respect to the former case, the consumption of sodium is lowered (its abundance does not decrease at the end of the main sequence). As a consequence the abundances of ^{24}Mg and of the total magnesium do not increase although one does not obtain the decrease required by the observations. Finally the ^{26}Mg burning is favored so that aluminum is produced earlier on the main sequence although its final abundance reaches the same value as in model 60rA.

In summary the new set of nuclear reactions resolves partly the difficulties encountered by model 60rA regarding the anticorrelation between Mg and Al. However the predicted magnesium isotopic ratios are still in conflict with the data by Yong et al. (2003, 2005).

3.4. NeNa and MgAl predictions with experimental extreme values - Model 60rC

In order to try and solve the remaining difficulties, we look now for the most favorable set of nuclear reactions by considering the

⁴ The abundance of the unstable isotope ^{26}Al which decays into ^{26}Mg is included in the total ^{26}Mg abundance.

published experimental limits. In model 60rC (set C) we make the following assumptions (see Table 2): We take the lower limits for the burning rates of all the neon isotopes in order to lower the overall production of sodium. We also take the lower limit for the $^{23}\text{Na}(p, \gamma)$ reaction which becomes now the slowest reaction of the NeNa chain. This reduces the linkage between the two chains and disfavors the production of ^{24}Mg . Regarding the MgAl chains, we take the upper limits for the destruction rates of the magnesium isotopes and the lower limits for the burning rates of ^{27}Al .

The corresponding predictions are shown by the short-dashed lines in Fig. 3. The overall increase of the ^{23}Na abundance is more modest than in the previous models. One obtains now an important decrease of the ^{26}Mg abundance, while the final predictions for ^{25}Mg and ^{27}Al are essentially not affected with respect to sets A-B. Again, ^{24}Mg stays constant during the hydrogen-burning phase. Nevertheless the total magnesium abundance decreases by 0.1 dex in this case. The stronger variation observed could come from more massive stars where the central temperature is hotter and the burning rate of ^{24}Mg is faster (see § 5).

3.5. Model 60rD

As shown previously the difficulty regarding the Mg destruction comes mainly from the fact that the central temperature reaches the required extreme values only at the very end of the main sequence (see Fig. 7). We thus note that the use of the rate published for the $^{24}\text{Mg}(p, \gamma)$ reaction Powell et al. (1999) is not compatible with significant Mg depletion within the core of massive main sequence stars. This led us to tentatively modify this rate in order to reconcile the theoretical predictions with the abundance data.

In model 60rD we keep all the reaction rates as in 60rC except for the burning rate of ^{24}Mg that we artificially enhance by a factor of 10^3 and $10^{1.5}$ at 50 and 60×10^6 K respectively (the recommended rate is used for temperature lower than 40×10^6 K and higher than 70×10^6 K). With these assumptions this reaction becomes as efficient as the other ones involved in the MgAl chain (see the arrows on Fig. 2).

As a result (see the dotted lines in Fig. 2) the ^{24}Mg abundance decreases by about 0.4 dex when the central hydrogen mass fraction equals ~ 0.2 . At the end of the main sequence ^{25}Mg and ^{26}Mg are respectively slightly destroyed and produced. Simultaneously the total magnesium abundance decreases by 0.3 dex while that of ^{27}Al increases by 1.2 dex for a central hydrogen mass of 0.2. These predictions are in good agreement with the observational constraints.

3.6. Summary

Our models were computed with the metallicity of NGC 6752 ($[\text{Fe}/\text{H}]=-1.5$) with the aim of comparing our theoretical predictions with the observations in this GC. In this section we have focused on the nucleosynthesis within the core of a $60 M_{\odot}$ main sequence star. The corresponding abundance variations are thus the most extreme ones one might expect, and they cannot be compared directly with the observational data. However we see already that we hold a serious candidate for building up the observed inhomogeneities and that it is worthwhile to explore further the WFRMS scenario.

The situation can be summarized by a close inspection of Table 4 where we list the most extreme abundance variations be-

Table 4. Mean core abundance variations during MS of the 60 M_{\odot} models. δX refers to the amplitude (in dex) of variation of element X. For NGC 6752 it refers to the amplitude variation observed between polluted and unpolluted stars

Model	δC	δN	δO	δNa	δMg	δAl
NGC 6752	-0.7	1.7	-1.0	0.9	-0.3	1.4
60rA	-0.9	1.5	-1.8	1.6	0.5	0.7
60rB	-0.9	1.5	-1.8	1.6	0.0	0.7
60rC	-0.9	1.5	-1.8	1.0	-0.1	0.7
60rD	-0.9	1.5	-1.8	1.0	-0.4	1.3

tween polluted and unpolluted stars in NGC 6752 as well as in the core of our 60 M_{\odot} models. We see that the comparison is rather favorable as far as the O-Na anticorrelation is concerned and that sets A and B lead to higher Na production than set C. On the other hand, the Mg-Al anticorrelation appears to be more difficult to reproduce. The use of sets A and B lead to a Mg-Al correlation, while that of set C builds up a weak Mg-Al anticorrelation. The situation becomes however more favorable when one increases the rate of the $^{24}Mg(p, \gamma)^{25}Al$ reaction as in model 60rD. In that case ^{24}Mg is destroyed while the abundance of ^{25}Mg is barely affected and that of ^{26}Mg slightly increases. This is in agreement with the observational constraints obtained on the Mg isotopes in NGC 6752 stars by Yong et al. (2005).

Let us note that the H-burning signatures we describe are similar to those found in the H-burning shell during central He-burning. Indeed in this shell the temperature does not surpass 60×10^6 K. Also the situation is not very different in rotating and non rotating models, the central temperatures and densities being weakly affected by rotation.

This study emphasizes the importance of some reactions: proton-captures on ^{20}Ne and ^{23}Na respectively govern the amount of sodium produced and the linkage between the NeNa and MgAl chains. Concerning the MgAl chain, the key reaction is the proton-capture on ^{24}Mg . A raise of its rate with respect to the published values is required to reproduce the extreme variations of magnesium and aluminum in the central region of a 60 M_{\odot} star. This is due to the fact that the required temperature (of about $72\text{--}78 \times 10^6$ K, see Prantzos & Charbonnel in preparation) is reached in the stellar core only at the very end of the main sequence in this object (see Fig. 7).

4. Mixing and ejection of matter in a rotating 60 M_{\odot} star

In the previous section we discussed what happens from the nucleosynthetic point of view in the core of a (rotating or non-rotating) 60 M_{\odot} star. We will now describe the critical effects of rotation on stellar mass loss and internal chemical structure. Finally we will follow the evolution of the surface abundances and compare our predictions with the data in GC stars.

4.1. Mass loss

Fig. 4 shows the evolution with time of the ratio between the surface and the break-up velocity in our 60 M_{\odot} model with $V_{ini} = 800 \text{ km s}^{-1}$. This ratio lies around 0.95 at the beginning of the main sequence. Rapidly, it falls down to 0.91 due to the establishment of differential rotation in the star: during this initial phase angular momentum is carried from the external regions into the internal layers and the core accelerates (see Meynet & Maeder 2000). Later on Ω/Ω_{crit} increases up to

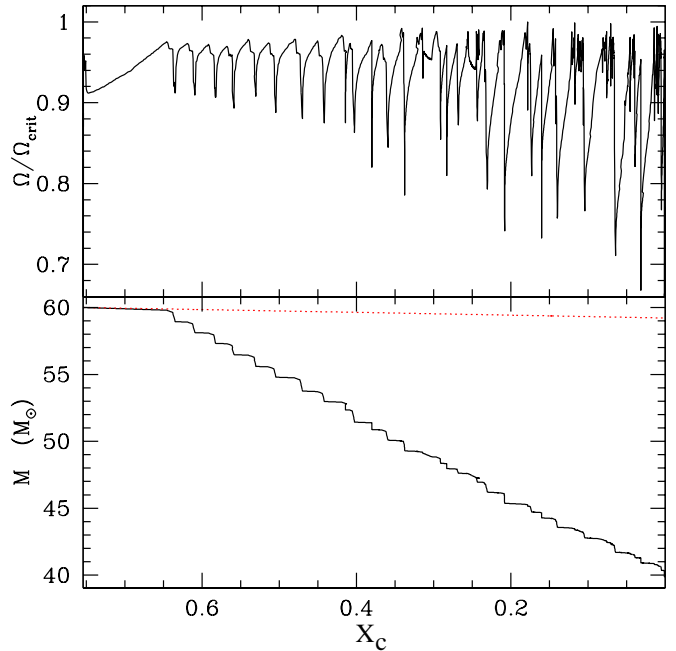


Fig. 4. (top) Ratio of the surface rotation velocity to the break-up value for model 60rC. (bottom) Evolution of the total stellar mass for models 60rC and 60sC (full and dotted lines respectively) along the main sequence (the abscissa is the central mass fraction of hydrogen)

reach unity (see § 2). However we force the model to stay below this level in order to avoid numerical difficulties (see § 2.2). Fig. 4 shows that all the episodes of strong mass loss correspond to a decrease of the surface velocity below the critical value. Then surface rotation velocity raises again. This process probably leads to the formation of a circumstellar disk. We make the hypothesis that this material is eventually lost by the star.

During the whole main sequence mass loss is dominated by this strong rotation-induced mechanical wind and is increased by more than a factor of 24 with respect to the standard case (e.g., model 60rC loses 20 M_{\odot} whereas the non rotating model expels less than 1 M_{\odot}).

As we just described, fast rotation does change the stellar mass loss *quantitatively*. But it has also a crucial *qualitative* impact on the properties and the topology of the ejecta. Indeed when the star rotates close to or at break-up the centrifugal force balances gravity. As a result, the mass loss is at least partly mechanically-driven, and the equatorial matter is released into a Keplerian disk. Very likely an equatorial disk forms as observed around Be stars (e.g., Porter & Rivinius 2003). This ejected material will thus be very easily retained within the GC potential well. This is very different from the non-rotating situation where the radiative winds escape at high velocity. This is one of the key points of our scenario which will be discussed in detail in § 7.

As explained in § 2.2 the model evolves away from the Ω -Limit when it leaves the MS. At that moment however the most massive stars ($M \geq 60 M_{\odot}$) encounter the $\Omega\Gamma$ -Limit. In the present work, we suppose that the matter lost at the $\Omega\Gamma$ -Limit is released in an equatorial disk, as in the case of the material lost at the Ω -Limit. When the star moves away from the $\Omega\Gamma$ -Limit due to heavy mass loss, the radiatively-driven fast winds take over.

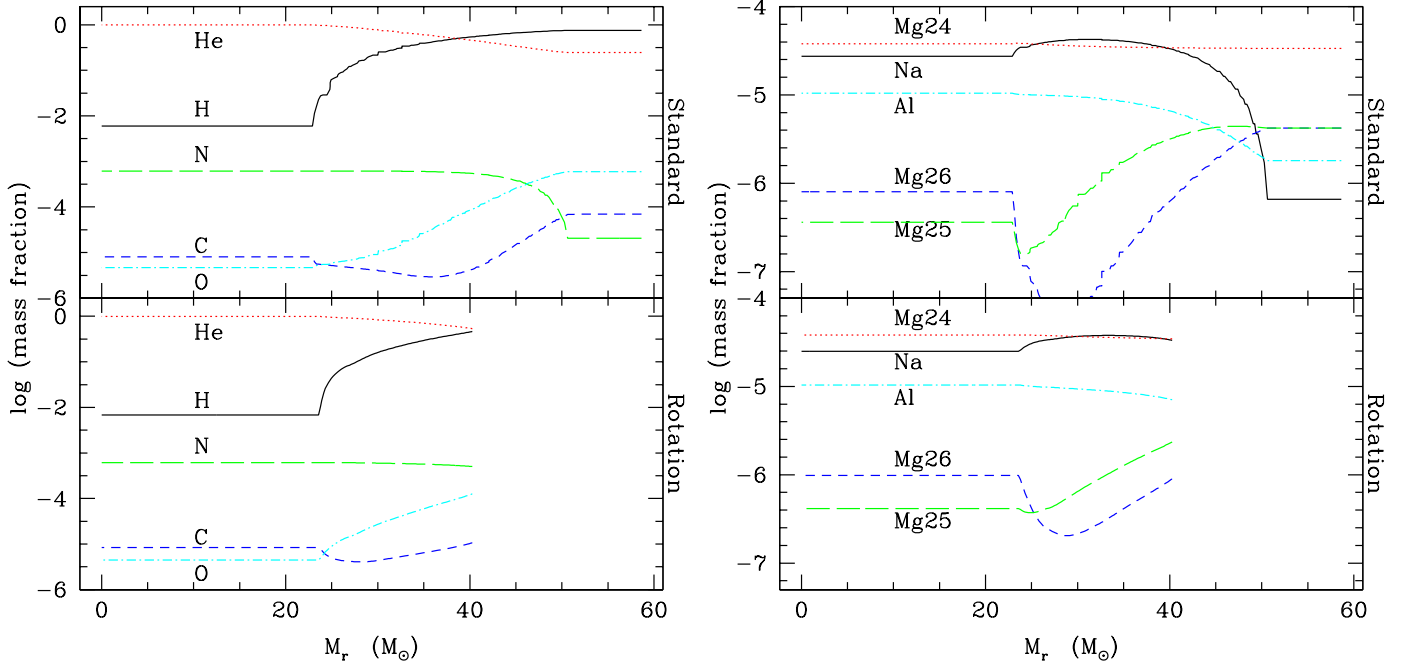


Fig. 5. Abundance profiles at the end of main sequence ($X_c \approx 0.01$) for the $60 M_\odot$ models in the standard case (model 60sC, top) and for $V_{\text{ini}} = 800 \text{ km s}^{-1}$ (model 60rC, bottom)

4.2. Abundance profiles

Since mass loss is very efficient in the rotating case, the star peels off revealing the H-processed layers at the surface. Rotational mixing strengthens the modifications of the surface abundances as the products of central burning are transported outwards by various instabilities induced by rotation.⁵

In Fig. 5 we show the abundance profiles of various chemical elements as a function of the Lagrangian mass for the $60 M_\odot$ star (computed using set C for the nuclear network) at the end of the main sequence in the standard and rotating models ($V_{\text{ini}} = 0$ and 800 km s^{-1} respectively). In both cases the size of the convective core is very similar (respectively 23.7 and $23.5 M_\odot$ in the standard and rotating models at the end of the main sequence) as well as the final central abundances (the central temperature differs by less than 1% between the two models).

Outside the convective core however the abundance profiles show some notable differences. The most striking effect is due to mass loss which is strongly enhanced in the rotating model. The induced strong “peeling” exposes the nuclear regions. As a consequence the surface abundances and wind at the end of the main sequence hold the signatures of H-processing.

4.3. Composition of the ejecta

During the evolution of our $60 M_\odot$ rotating models we can distinguish the following phases:

1. The very beginning of the main sequence during which the surface velocity approaches the critical limit (between $X_c \sim 0.76$ to 0.65 in Fig. 4).
2. The rest of the main sequence when the surface velocity is at (or very near) the critical limit (for X_c below 0.65 in Fig. 4).
3. The beginning of the core He-burning phase when the stellar luminosity is close to the Eddington value and the surface velocity stays close to the $\Omega\Gamma$ -Limit.
4. The end of the He-burning phase. From this moment on the star is away from the $\Omega\Gamma$ -Limit and the mass loss is mainly radiatively-driven.

During the phases 2 and 3 described above, mass loss is mainly mechanically-driven and the stellar winds are supposed to be slow; they are enriched in H-burning products only. When the phase 4 starts the stellar surface and the ejecta are enriched in both H-burning and He-burning products, the winds are fast.

Fig. 6 presents the evolution of the surface abundances in the rotating $60 M_\odot$ models as a function of the remaining stellar mass from the zero age main sequence up to the end of central He-burning; the different lines correspond to models computed with the various sets of nuclear reactions described in § 2.1 (60rA, B, C and D). We also indicate the range of abundances exhibited by the low-mass stars in NGC 6752 (shaded boxes).

The surface abundance variations do mimic the central ones (see Fig. 3 and the discussion in § 3) with some delay due to non-instantaneous rotational mixing. In all the cases the surface abundances of carbon and oxygen at the end of the main sequence fall respectively by 0.9 and 1 dex with respect to their original values, whereas that of nitrogen raises by 1.5 dex. The sodium surface abundance increases by 0.8 or 1.6 dex depending on the assumed nuclear reaction rates. Aluminum increases in all the cases but in a more efficient way when one enforces ^{24}Mg -burning by increasing significantly the corresponding reaction rate (set D). In summary and as discussed previously, the O-Na anticorrelation naturally shows up in all the cases. However one

⁵ The most important ones are the meridional currents and the shear turbulence (see the review by Talon 2004). The inclusion of these transport mechanisms has improved the massive star models in many respects (see Maeder & Meynet 2000 for references); in particular, rotating models can reproduce the chemical enrichment observed at the surface of OBA stars (Heger & Langer 2000; Meynet & Maeder 2000).

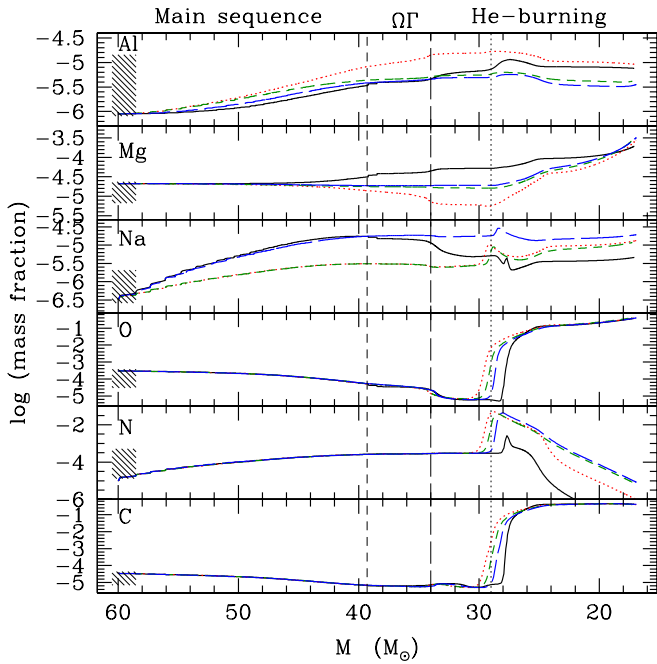


Fig. 6. Evolution of the surface abundances as a function of remaining mass for the $60 M_{\odot}$ rotating models computed with various sets of nuclear reactions : set A (full line), set B (long dashed lines), set C (short dashed lines) and set D (dotted lines). The short-dashed vertical line indicates the end of the main sequence. The $\Omega\Gamma$ -Limit phase is located between the short- and long-dashed lines. The dotted line marks the moment when He-burning products start to appear at the surface. The shaded boxes on the left indicate the amplitudes of the abundance variations observed at the surface of low-mass stars in NGC 6752.

has to call for an increase of the $^{24}\text{Mg}(p,\gamma)$ reaction rate in order to correctly build up the Mg-Al anticorrelation.

The H-burning signatures are reinforced at the stellar surface at the beginning of the central He-burning phase mainly as a result of previous mass loss episodes.

However later on the products of He-burning start to show up at the surface. In particular the oxygen abundance raises steeply from 10^{-5} to nearly 0.6 in mass fraction when the total stellar mass is lower than $\sim 28 M_{\odot}$. C and N also display strong enhancement at this phase. After the abundance of nitrogen decreases being transformed into ^{22}Ne .

In summary the ejecta of fast rotating massive stars display the chemical patterns observed in GC stars both on the main sequence and during the $\Omega\Gamma$ -Limit phase. Importantly, these are exactly the phases where matter is ejected by gently blowing winds which can be easily retained within the GC potential well. At the opposite, the He-burning products are released in the interstellar matter through fast radiatively-driven winds. We will come back to that crucial point of the WFRMS scenario in the discussion.

4.4. Effect of the initial rotation velocity

In order to investigate the impact of the initial rotation velocity on the overall predictions we have computed a $60 M_{\odot}$ model with an initial velocity of 600 km s^{-1} (model 60rE, with set C) instead of 800 km s^{-1} (model 60rC). The mixing of chemicals is less efficient in the slowest model as the shear turbulence, which dominates the transport processes, decreases with lower angu-

lar velocity. However model 60rE reaches the break-up velocity later during the main sequence (when the central hydrogen mass fraction is 0.4 instead of 0.65 in model 60rC). Both effects tend to compensate each other: the mixing has a smaller efficiency but has more time to act before the star reaches the break-up. This leads to abundance variations which are even more pronounced. As an example the nitrogen abundance in winds when break-up is reached is 55% higher in model 60rE than in model 60rC (see Table 5).

When the stars are at break-up, the mass loss rate is higher for a lower initial rotation velocity: compared to the standard (non-rotating) case it is 29 and 24 times higher in models 60rE and 60rC respectively. The total stellar mass at the end of the main sequence is higher (by $\sim 3 M_{\odot}$) in model 60rC. These differences play only a minor role for the composition of the yields which differ by only a few percents between the two models.

Let us note finally that with an initial velocity around 300 km s^{-1} the $60 M_{\odot}$ star would fail to reach the break-up and the conditions for the WFRMS scenario would not be fulfilled. If we infer models with various initial mass and metallicity (Ekström et al, in preparation), the $60 M_{\odot}$ would reach the critical velocity with initial velocity as low as 400 km s^{-1} . However fast rotation is possibly a characteristic of massive stars in a very dense environment such as forming GC where multiplicity and stellar collisions can play an important role. This point is discussed in more detail in § 7.

4.5. Summary

To sum-up, the WFRMS appears to be very promising. Rotational mixing efficiently transports elements from the convective core to the surface. A high initial rotation velocity allows the star to reach break-up early on the main sequence and to eject important quantities of material loaded with H-burning products. This material is probably ejected through a slow wind and has great chance to remain in the GC potential well (see § 7).

The abundance patterns at the stellar surface and in the ejecta follow those created in the core with some delay. The amplitude of the predicted O-Na anticorrelation reproduces well the observational feature. Although the $60 M_{\odot}$ star produces too few Al when one sticks to the nuclear experimental value for the $^{24}\text{Mg}(p,\gamma)$ reaction rate, an increase of this rate allows one to explain the observed Mg-Al anticorrelation.

5. Dependence on the initial stellar mass

Let us now discuss how the theoretical predictions depend on the initial stellar mass. Standard and rotating models with initial masses ranging between 20 and $120 M_{\odot}$ are presented; in all the cases we used the set C for the nuclear reaction rates.

5.1. Nucleosynthesis and mixing

The initial mass has a direct effect on nucleosynthesis through the changes in the central temperature (see Fig. 7). As a result the NeNa and MgAl chains are more active in the warmer convective core of more massive stars.

The evolution along the main sequence of the central abundances of some interesting nuclei is shown in Fig. 8 for the 20 and $120 M_{\odot}$. It can be compared to Fig. 3. The following differences can be noted:

- The CNO equilibrium value of O is slightly lower in the higher temperature regime of the $120 M_{\odot}$ stellar model.

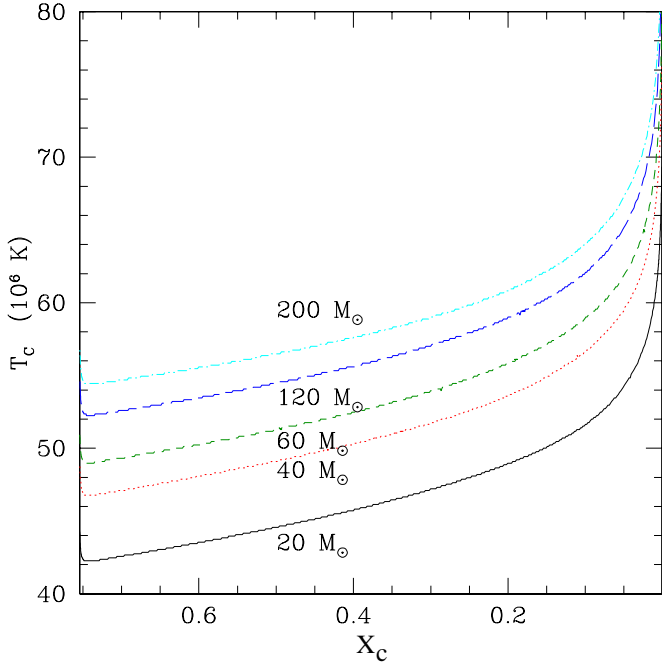


Fig. 7. Evolution of the central temperature for the 20, 40, 60, 120 and 200 M_{\odot} rotating stars as a function of the central hydrogen abundance during the main sequence.

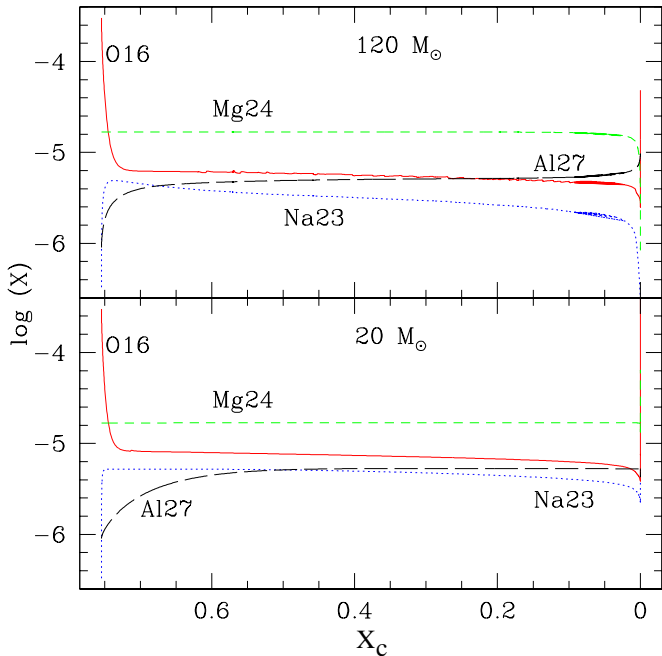


Fig. 8. Evolution of the central abundances of ^{16}O , ^{23}Na , ^{24}Mg and ^{27}Al as a function of the central hydrogen abundance on the main sequence for the 20 and 120 M_{\odot} rotating models.

- ^{23}Na is first produced to the same extent in both models, but later on it decreases faster in the more massive star.
- In the 120 M_{\odot} model ^{24}Mg decreases by 1.2 dex at the very end of the H-burning phase, while the 20 M_{\odot} never reaches sufficiently high temperatures for this element to burn.

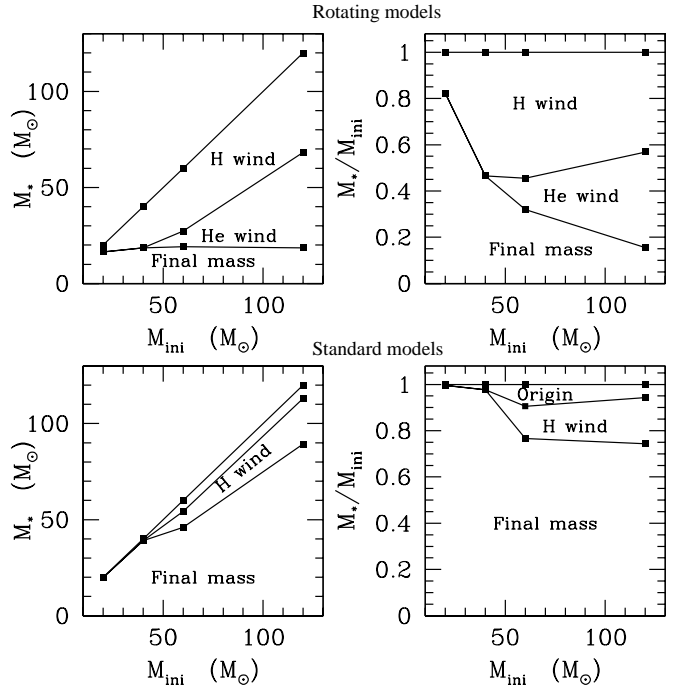


Fig. 9. Composition of the matter ejected in the winds as a function of initial stellar mass for the rotating and standard models (upper and lower panels respectively). The ejecta are presented in solar mass (left) or scaled with respect to initial mass (right). The winds enriched in H- and He-burning products are quoted respectively as “H wind” and “He wind”. “Origin” refers to matter which is not modified by nuclear burning. “Final mass” indicates the mass of the stars at the end of central He-burning.

- ^{27}Al is produced earlier in the 120 M_{\odot} model. Nevertheless the plateau stays at the same level in both models. Only at the very end of the main sequence, does the Al abundance rapidly increase in the more massive star as a result of ^{24}Mg burning.

Thus the main relevant difference between both stars concerns the MgAl chain. Only in the 120 M_{\odot} model and at the very end of central H-burning are ^{24}Mg and ^{27}Al respectively destroyed and produced. Even the 200 M_{\odot} star does not reach central temperature high enough to convert ^{24}Mg before the very end of main sequence.

As discussed in Meynet & Maeder (2000), rotational mixing is more efficient when the initial stellar mass is higher, favoring the transport of the nuclear products outwards. At a given evolutionary stage, more massive stars also present stronger winds, both radiatively- and mechanically-induced.

5.2. Winds

Fig. 9 illustrates the differences between the standard and rotating models for the wind composition and the remaining stellar mass at the end of central He-burning. As already discussed, the rotating models lose much more mass than the standard ones due to three reasons: first, they do undergo mechanical winds when they reach the break-up velocity; second, their radiatively-driven winds are enhanced by the correcting factor due to rotation; third, they enter the WR phase earlier in their evolution.

The rotating models with an initial mass above 40 M_{\odot} lose about half of their mass through winds loaded in H-burning

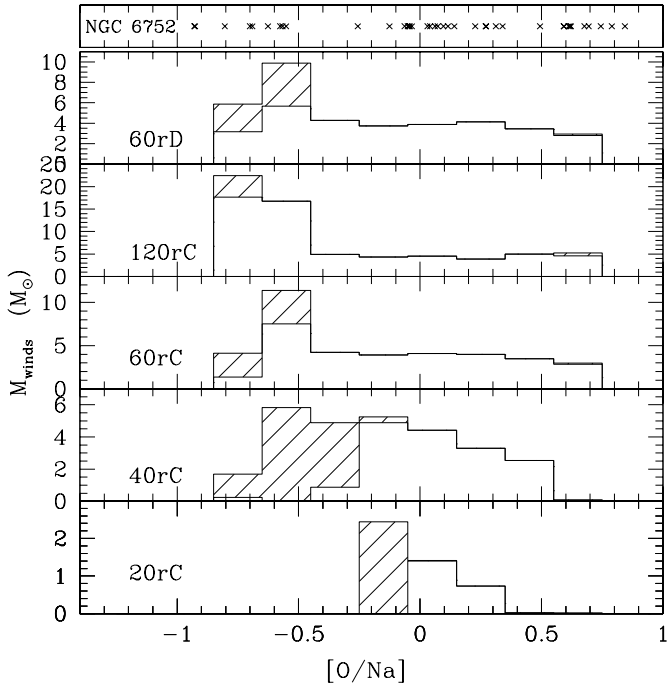


Fig. 10. (Top) Crosses are observed $[O/Na]$ ratio in individual NGC 6752 stars computed from the data of Grundahl et al. (2002) and Yong et al. (2003). (Other panels) Theoretical histograms built from the wind composition of rotating massive stars in which 30% of pristine matter is added as required by the Li behavior (see the text). The white and shaded areas indicate respectively the slow (i.e., when the star is at breakup) and fast winds

products. Moreover this matter is released very smoothly in the interstellar medium, with velocities low enough to remain in the GC. This is not the case of the winds of non-rotating massive stars. Indeed in that case, the wind velocities on the main sequence are of the order of 1000 to 2000 km s⁻¹ (see e.g. Lamers et al. 1995) and this material is probably thrown off the gravitational potential well of the cluster.

6. Comparison with observed abundance variations in GCs

Here we explore how the ejecta of massive rotating stars can be used to form low-mass stars displaying abundance variations in light elements. It is out of the scope of the present paper to present a detailed study of the interaction between the disk enclosing fast rotating massive stars and the surrounding proto-cluster gas. We will thus only make some simple assumptions to verify if massive stars can be the progenitors of the long-lived stars we observe today.

As the disks may be mixed with some pristine gas, we need first to evaluate the amount of this dilution. For that we use abundance variations in Li measured by Pasquini et al. (2005) in NGC 6752: Li is found to be as low as $A(Li) = 1.93$ (Alonso temperature scale) in the most polluted stars. In the present models we do not follow explicitly the nucleosynthesis of lithium but we can reasonably assume that this fragile element is completely destroyed due to high temperature in the stellar interior and to the strong mixing induced by rotation. If we assume that the initial lithium abundance of the intracluster gas corresponds to the cosmological value of 2.61 (Coc et al. 2004) and that no lithium is

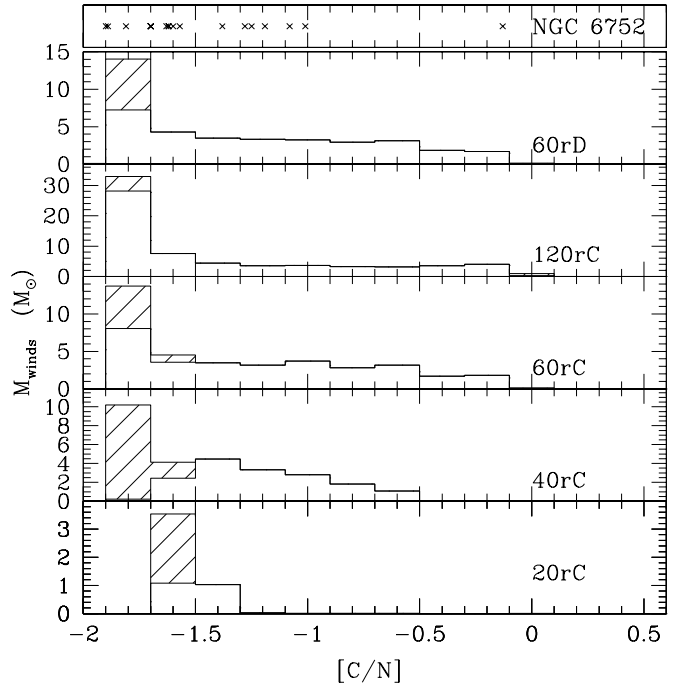


Fig. 11. Same as Fig. 10 for $[C/N]$ ratio (data from Carretta et al. 2005)

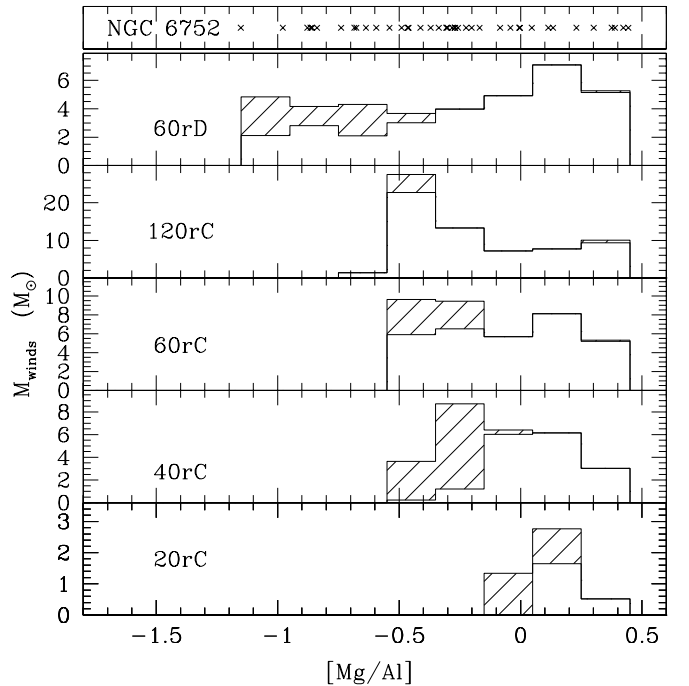


Fig. 12. Same as Fig. 10 for $[Mg/Al]$ ratio (data from Grundahl et al. 2002; Yong et al. 2003)

present in the wind of massive stars, we need to add about 30% of pristine gas to those winds in order to find the extreme value of lithium (see also Prantzos & Charbonnel in preparation).

As a first estimate we use this dilution factor between the stellar winds and the original matter and check whether it allows to reproduce all the observed abundance variations. In real proto-globular cluster there will surely be a dispersion in the amount

of dilution which in turn creates a variation in the abundances of low-mass stars.

Fig. 10, 11 and 12 display the composition of the mixed matter formed by adding 30% of pristine gas to massive star ejecta as well the observed abundance distributions in NGC 6752 (Grundahl et al. 2002; Yong et al. 2003; Carretta et al. 2005). The theoretical histograms indicate the mass ejected by winds mixed with pristine gas resulting on a given chemical composition. The white areas correspond to the mass lost at break-up, while the hatched regions indicate that the corresponding winds are released when stellar rotation is well below its critical value (this occurs at the very beginning of the main sequence and during the He-burning phase). This latter component has thus a high velocity and probably escapes the GC potential well. Only the H-rich loaded winds are shown here. The He-rich winds are released at high velocity and are supposed to escape the potential well of the GC.

Let us first concentrate on the [O/Na] distribution. The abundance pattern in the mixed matter of the 60 and 120 M_{\odot} models covers the entire observational range. The case of the less massive stars is different. At first glance the predictions for the 40 M_{\odot} model also account well for the observed dispersion. This is not the case when one considers only the slow winds ejected at break-up. The 20 M_{\odot} star follows the same trend but with a smaller extent. Let us note that the highest [O/Na] ratio for both the 20 and 40 M_{\odot} stars is shifted to the left compared to more massive models. This is due to the longer time required to reach critical velocity at the beginning of the main sequence. When the break-up is reached rotational mixing had more time to transport the elements through the radiative envelope.

Turning our attention to the [C/N] distribution (Fig. 11) we find that the ejecta of rotating massive stars cover very nicely the observational range. Again the 20 M_{\odot} and 40 M_{\odot} , being more mixed before reaching break-up, do not expel matter with original composition (see Table 5).

Regarding the [Mg/Al] ratio we see that the winds of all the models computed with the set C (experimental limits) present lower abundance variations than required by the observed distribution. In addition let us recall that the magnesium isotopic ratios obtained in these models are at odd with the observed ones: even in the case of the 120 M_{\odot} aluminum is built mainly from ^{25}Mg and ^{26}Mg . Only model 60rD covers the whole observational range both in terms of Mg and Al abundances and of Mg isotopic ratios. The same would be true for other masses computed with set D. This difficulty remains even in the extreme case, where present day halo stars would be naked cores of massive stars having undergone strong evaporation at the end of the main sequence. Only at the end of main sequence the 60 and 120 M_{\odot} models manage to destroy ^{24}Mg by more than 0.3 dex and to enhance ^{27}Al . However at that time the high central temperature leads to a strong destruction of ^{23}Na which falls near or under its initial value.

7. Discussion

Let us now discuss some details of the WFRMS scenario.

7.1. Kinematics and topology of the ejected material

Figure 13 shows the distribution of the globular clusters as a function of the escape velocity estimated at the center and at half-mass radius of the present-day cluster (continuous and dotted line respectively, Gnedin et al. 2002). One sees that more

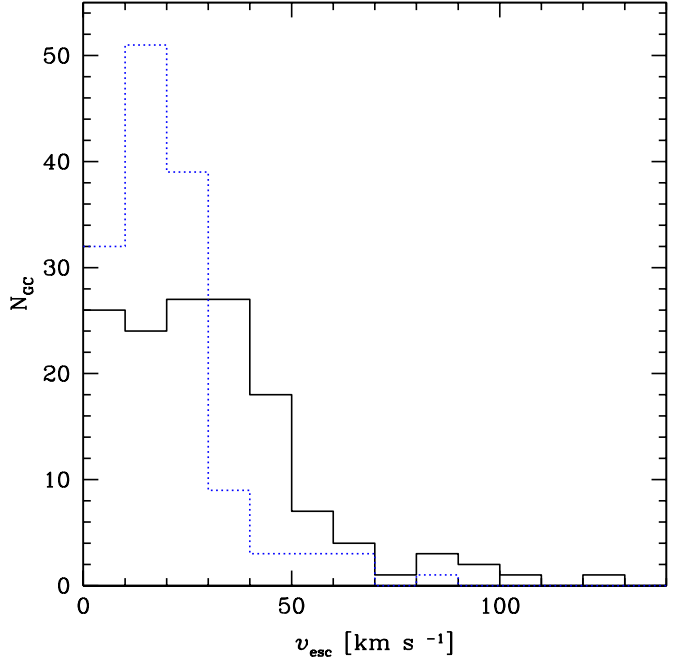


Fig. 13. Histogram of the number of globular clusters having a given value of the escape velocity. The data are taken from Gnedin et al. (2002). The continuous line shows the results for the escape velocity at the center of the cluster, the dotted line at the cluster half-mass radius.

than 60% of the 141 globular clusters used to build the histogram (*i.e.* the large majority of the known galactic globular clusters) have an escape velocity at the center between 20 and 100 km s^{-1} . The range is shifted to lower values if escape velocities estimated at half-mass radius are used. Thus, taken at face, these values imply that all the wind ejecta of O-type stars and of WR stars (wind velocities of a few thousandths of km s^{-1}), of Luminous Blue Variable (wind velocities of a few hundred km s^{-1}) as well as the supernova ejecta (velocities of the order of 10 000 km s^{-1}) will be lost by the globular cluster. This statement must however be a little tempered by a couple of facts: first the escape velocity of the present day globular clusters may be different from the one at the time of their formation. Would the present globular clusters be the remnants of much more massive systems having lost a great part of their initial mass, then the present day escape velocity might be a poor estimate of the escape velocity at the time of their formation.⁶ Second, the interstellar medium at the time of the globular cluster formation was much more dense and thus the matter ejected was slowed down by the bow shock between the ejecta and the ambient medium as shown for instance in the numerical models by Freyer et al. 2003 (see also Garcia-Segura et al. 1996). It is however difficult, without a more precise view of the initial conditions of the globular cluster formation to come to firm conclusion on these points.⁷ In

⁶ More precisely we need here the escape velocity at the time of the chemical inhomogeneities formation, which in our present model would be different from the time of formation of the first stellar generation.

⁷ Of course one could argue that we can observe young globular clusters and thus obtain some constraints on their formation. However, many (if not all) young super star clusters observed today and believed to be young globular clusters, result from galaxy merging or interactions. It is not clear at all that the old galactic globular clusters were formed in this way.

Table 5. Sum-up of the main features of our models: initial mass, initial surface velocity, and for each evolutionary phases the remaining mass and the mean mass fraction in the wind for several isotopes integrated from the zero age main sequence. The 20, 40 and 120 M_{\odot} models are computed with the reaction rates from set C. For rotating models the last division indicates abundance when He-burning products appear at the surface, or at the end of He-burning phase depending on the first case reached.

M_{ini} M_{\odot}	V_{ini} km s^{-1}	M_{f} M_{\odot}	H1	He4	C12	N14	O16	F19	Na23	Mg24	Mg25	Mg26	Al27
Mean mass fraction in winds													
STANDARD MODELS													
End of central H-burning													
20	0	19.9	7.5e-1	2.4e-1	3.5e-5	1.0e-5	3.0e-4	1.5e-8	3.3e-7	1.7e-5	2.1e-6	2.1e-6	9.0e-7
40	0	39.7	7.5e-1	2.4e-1	3.5e-5	1.0e-5	3.0e-4	1.5e-8	3.3e-7	1.7e-5	2.1e-6	2.1e-6	9.0e-7
60	0	59.2	7.5e-1	2.4e-1	3.5e-5	1.0e-5	3.0e-4	1.5e-8	3.3e-7	1.7e-5	2.1e-6	2.1e-6	9.0e-7
120	0	117.0	7.5e-1	2.4e-1	3.5e-5	1.0e-5	3.0e-4	1.5e-8	3.3e-7	1.7e-5	2.1e-6	2.1e-6	9.0e-7
End of central He-burning													
20	0	19.9	7.5e-1	2.4e-1	3.5e-5	1.0e-5	3.0e-4	1.5e-8	3.3e-7	1.7e-5	2.1e-6	2.1e-6	9.0e-7
40	0	39.1	7.5e-1	2.5e-1	3.5e-5	1.0e-5	3.0e-4	1.5e-8	3.3e-7	1.7e-5	2.1e-6	2.1e-6	9.0e-7
60	0	45.9	6.9e-1	3.1e-1	2.6e-5	7.9e-5	2.3e-4	1.2e-8	1.2e-6	1.7e-5	1.6e-6	1.7e-6	1.8e-6
120	0	89.3	5.9e-1	4.1e-1	1.5e-5	1.7e-4	1.4e-4	6.3e-9	2.0e-6	1.7e-5	9.9e-7	1.2e-6	3.0e-6
ROTATING MODELS													
Break-up reached													
20	600	20.0	7.5e-1	2.4e-1	1.1e-5	4.9e-5	2.9e-4	1.5e-8	7.5e-7	1.7e-5	2.1e-6	2.2e-6	9.3e-7
40	800	40.0	7.5e-1	2.4e-1	3.5e-5	1.3e-5	3.0e-4	1.6e-8	3.7e-7	1.7e-5	2.1e-6	2.2e-6	9.2e-7
60rE	600	59.7	7.5e-1	2.5e-1	3.3e-5	1.7e-5	3.0e-4	1.5e-8	4.2e-7	1.7e-5	2.1e-6	2.1e-6	9.2e-7
60rA	800	59.9	7.5e-1	2.4e-1	3.5e-5	1.1e-5	3.0e-4	1.6e-8	3.5e-7	1.7e-5	2.1e-6	2.1e-6	9.2e-7
60rB	800	59.9	7.5e-1	2.5e-1	3.5e-5	1.1e-5	3.0e-4	1.6e-8	3.5e-7	1.7e-5	2.1e-6	2.2e-6	9.2e-7
60rC	800	59.9	7.5e-1	2.4e-1	3.5e-5	1.1e-5	3.0e-4	1.6e-8	3.4e-7	1.7e-5	2.1e-6	2.2e-6	9.2e-7
60rD	800	59.9	7.5e-1	2.5e-1	3.5e-5	1.1e-5	3.0e-4	1.6e-8	3.4e-7	1.7e-5	2.1e-6	2.2e-6	9.2e-7
120	800	119.5	7.5e-1	2.4e-1	3.5e-5	1.1e-5	3.0e-4	1.6e-8	3.4e-7	1.7e-5	2.1e-6	2.1e-6	9.2e-7
End of central H-burning													
20	600	18.4	7.3e-1	2.7e-1	1.6e-6	8.8e-5	2.5e-4	1.3e-8	1.5e-6	1.7e-5	1.8e-6	2.0e-6	1.3e-6
40	800	28.8	7.2e-1	2.8e-1	1.3e-5	9.3e-5	2.3e-4	1.2e-8	1.4e-6	1.7e-5	1.7e-6	1.9e-6	1.6e-6
60rE	600	42.7	6.7e-1	3.3e-1	1.9e-5	1.1e-4	2.1e-4	1.0e-8	1.5e-6	1.7e-5	1.5e-6	1.6e-6	2.0e-6
60rA	800	39.9	6.8e-1	3.2e-1	1.9e-5	1.2e-4	2.0e-4	1.0e-8	7.1e-6	1.9e-5	1.4e-6	2.2e-6	1.5e-6
60rB	800	39.9	6.8e-1	3.2e-1	1.9e-5	1.2e-4	2.0e-4	1.0e-8	6.4e-6	1.7e-5	1.4e-6	2.0e-6	1.7e-6
60rC	800	39.7	6.8e-1	3.2e-1	1.9e-5	1.2e-4	2.0e-4	1.0e-8	1.7e-6	1.7e-5	1.4e-6	1.6e-6	2.1e-6
60rD	800	39.9	6.8e-1	3.2e-1	1.9e-5	1.2e-4	2.0e-4	1.0e-8	1.7e-6	1.6e-5	1.5e-6	1.8e-6	2.7e-6
120	800	76.6	6.1e-1	3.9e-1	1.7e-5	1.8e-4	1.3e-4	6.3e-9	2.2e-6	1.7e-5	9.2e-7	1.1e-6	3.1e-6
Appearance of He-burning products at the surface/End of central He-burning													
20	600	16.4	7.0e-1	3.0e-1	1.6e-6	1.1e-4	2.3e-4	1.1e-8	1.8e-6	1.7e-5	1.7e-6	1.9e-6	1.6e-6
40	800	18.5	5.7e-1	4.3e-1	9.3e-6	1.6e-4	1.6e-4	8.0e-9	2.1e-6	1.7e-5	1.2e-6	1.3e-6	2.7e-6
60rE	600	33.2	5.2e-1	4.8e-1	1.4e-5	1.7e-4	1.4e-4	7.2e-9	2.0e-6	1.7e-5	1.1e-6	1.2e-6	3.0e-6
60rA	800	30.8	5.4e-1	4.6e-1	1.5e-5	1.7e-4	1.5e-4	7.2e-9	8.6e-6	2.5e-5	1.3e-6	2.0e-6	2.5e-6
60rB	800	30.7	5.5e-1	4.5e-1	1.5e-5	1.7e-4	1.5e-4	7.2e-9	1.0e-5	1.7e-5	1.1e-6	1.5e-6	2.6e-6
60rC	800	30.7	5.5e-1	4.5e-1	1.5e-5	1.7e-4	1.5e-4	7.3e-9	2.0e-6	1.7e-5	1.1e-6	1.2e-6	3.0e-6
60rD	800	31.0	5.5e-1	4.5e-1	1.5e-5	1.7e-4	1.5e-4	7.3e-9	2.0e-6	1.4e-5	1.1e-6	1.6e-6	5.5e-6
120	800	68.7	5.0e-1	5.0e-1	1.5e-5	2.0e-4	1.1e-4	5.2e-9	2.2e-6	1.7e-5	8.4e-7	9.6e-7	3.5e-6

the following, in absence of a better knowledge of the globular cluster formation conditions, we shall consider that the present escape velocities are representative of the escape velocities at the time of the chemical inhomogeneities formation.

Thus we have to look if our massive star models are able to eject matter at sufficiently low velocities for allowing the ejecta to remain in the potential well of the globular cluster. Rotation might be of great help in this respect. Indeed, in situations where the surface equatorial velocity is such that the centrifugal acceleration exactly counterbalances the gravity, matter can be launched into a Keplerian orbit and an equatorial disk easily forms as schematically shown in Fig. 14. The material mainly “mechanically” ejected into the disc will be possibly available for further star formation, unless it falls back onto the star and/or is ejected outside the globular cluster by further violent wind episodes or by the supernova explosion. Let us briefly discuss these different possibilities:

– **Fall back of the disk material?** Be stars are main-sequence stars surrounded by a disc (Porter & Rivinius 2003). The ori-

gin of the disk is probably stellar rotation near the critical limit as convincingly discussed by Townsend et al. (2004). Thus these objects are exactly the observable counterparts of the stellar models we are interested in here. Observations (see the review by Rivinius 2005) indicate that Be star disks are eroded and finally dissipate, adding their material to the ambient interstellar medium. Thus these observations would favor the lost of the disk material around Be stars and not its fall back onto the star.

– **Ejection by fast stellar winds?** When the star does no longer rotate with the critical velocity, matter is no longer preferentially ejected in the equatorial plane, and different situations may occur. First it might be that the timescale for disk dissipation is very short and thus that most of the disk material has already disappeared when the faster radiatively driven winds set in. In that case there is the possibility that the fast wind pushes this freshly ejected material out of the globular cluster, which will be then lost. The most favorable case for keeping the material inside the globular cluster is

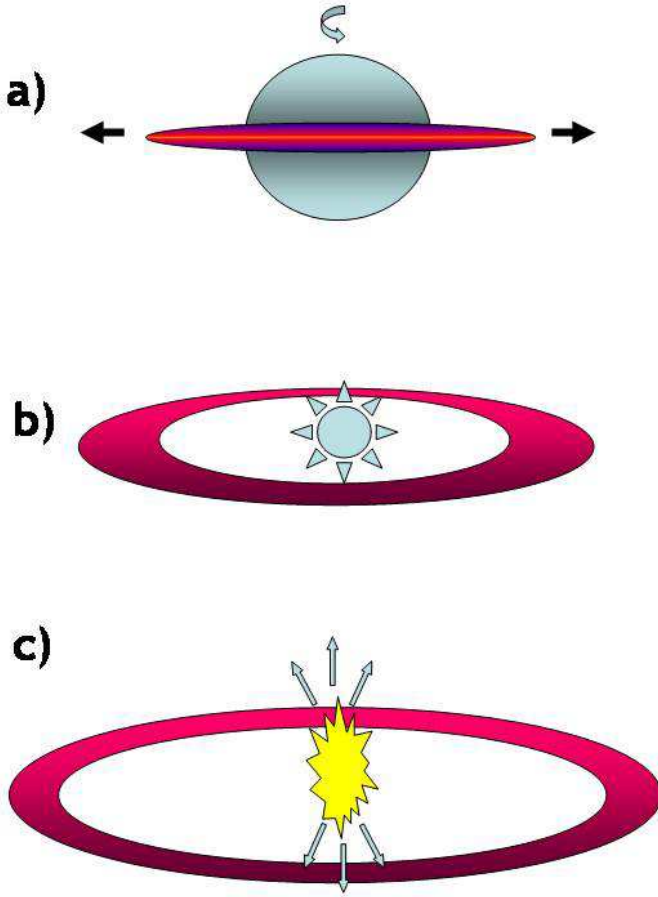


Fig. 14. Schematic view of the WFRMS scenario showing the possible geometry of the stellar ejecta at various evolutionary phases: **a)** during the main sequence, when the star rotates near or at the critical velocity, matter is preferentially ejected in the equatorial plane by the action of the centrifugal acceleration; **b)** after the main sequence, the surface velocity is no longer critical and the wind is triggered mainly by radiation. It is no longer equatorial and becomes isotropic; **c)** the supernova explosion resulting from an initially fast spinning star, if it occurs, may favor ejection through jets aligned along the rotational axis.

that the disk has a sufficiently long lifetime for still keeping most of its material when the fast winds set in. In that case, if the star is still in the blue part of the HR diagram (as is the case for our 60 and 120 M_{\odot}) and if its rotation is still sufficiently close to the critical value, the wind will be preferentially ejected along the rotational axis. This would thus prevent the winds to sweep off the disk. If the star has a rotational velocity well below the critical one, the wind is isotropic and one may hope that the fraction of the wind which may interact with the disk will be too small to destroy it (see Fig. 14).

- **Will the disk be thrown away by the supernova explosion?** In case a black hole is formed that swallows all the mass of the pre-supernova, no explosion occurs and the disk will not be affected. If, on the other hand, a supernova explosion occurs, the fast rotation of the core may favor ejection along the rotational axis as in the models of Maeda & Nomoto (2003). In that case there is some chance that the disk will not be affected by the supernova explosion as illustrated schematically in Fig. 14. Of course the disk ma-

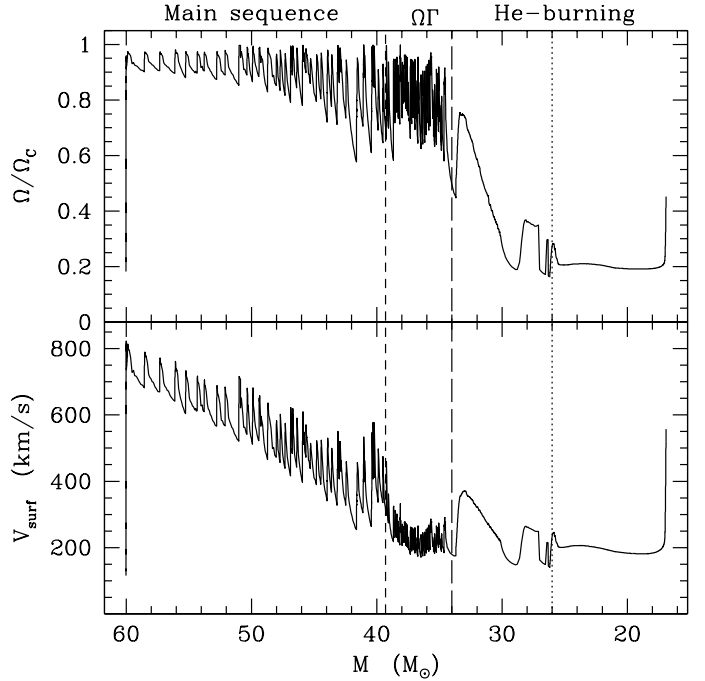


Fig. 15. Evolution of the ratio between the surface angular velocity and the classical critical velocity (top) and of the surface equatorial velocity (bottom) as a function of the remaining mass for the 60 M_{\odot} star. Vertical short-dashed line corresponds to the end of the main sequence and dotted line indicates the moment when He-burning products show up at the surface. The $\Omega\Gamma$ -Limit phase is delimited by the short- and long-dashed lines.

terial can also be destroyed and ejected out of the GC pushed away by the winds and/or supernova shocks from nearby massive stars. Our scenario will then be possible only if in relatively short timescales (shorter than typically the averaged time between two supernova events), new stars form in the disk, or more probably in the interaction region between the disk material and the interstellar medium. In that case, the fast moving material will escape following the nearly empty channels left behind by the star formation process, in line with the scenario proposed by PC06.

These ideas are highly speculative and will have to be checked by detailed hydrodynamical calculations in the future. For the purpose of the present discussion, we shall suppose that the equatorial disk formed when the star reaches the critical limit consists of material which will be made available for forming new stars in the globular cluster.

Now, in the frame of the above hypothesis, we have to see when this occurs during the evolution of our stellar models and whether sufficient mass with the adequate chemical composition is ejected during these phases. The present models show that the critical limit can be reached at two epochs:

1. During the main sequence, provided that the initial velocity is high enough. From Fig. 15 one sees that our 60 M_{\odot} model with $v_{\text{ini}} = 800 \text{ km s}^{-1}$ remains near the break-up limit during nearly the whole main sequence. At the turnoff, the star has lost more than 20 M_{\odot} .

2. After the main sequence we saw that stars massive enough do reach the $\Omega\Gamma$ -limit which maintains them at the break-up⁸ due to the raise of the luminosity. Strong mass loss ensues: During this phase the $60 M_{\odot}$ star expels more than $5 M_{\odot}$ (see Fig. 15). We suppose here that this material will still be preferentially ejected along the equatorial plane and will join the disk of slowly outflowing material.

7.2. Composition of the ejected material

In the previous sections we have seen that the chemical composition of the ejected material presents many similarities with the abundance patterns observed at the surface of globular cluster stars. If one focuses on the matter ejected during the main sequence, one sees however that the theoretical variations can account only partly for the observed range in oxygen and sodium. However slightly later in the evolution, strongly CNO processed material is ejected and the most extreme observational cases can be reproduced (see Table 5). The observed variations of Mg and Al can also be reproduced, provided the rate of the $^{24}\text{Mg}(p, \gamma)$ reaction is enhanced by about a factor 1000 for temperatures around 50×10^6 K. However if the non-enhanced rate for this reaction is correct, then our models reproduce only part of the Mg-Al anticorrelation.

One has to conclude that fast rotating massive stars are extremely good candidates for providing the material from which the long-lived low-mass stars that we are presently observing formed. Of course the process leading to the incorporation of this material in new stars is far from being described here, but at least we have given some reasons to believe that the interesting ejecta can be retained in the globular cluster. It has also to be stressed that the stars forming from the wind ejecta of massive stars mixed with some pristine interstellar gas would also present higher helium abundances (Salaris et al. 2006) and of course high C/N ratios. The values of the $^{12}\text{C}/^{13}\text{C}$ would be quite low: all the massive stars have ratio below 5. The corresponding implications will be studied in a subsequent work.

7.3. Why only in GCs?

To end this section, we can wonder why such a process did only occur in GCs. The environment of field halo stars is of course very different from the one of the globular clusters. However, in the past, they probably share, at least for a short time, a cluster environment. These clusters were probably much less massive and/or much less concentrated than the progenitors of the present day globular clusters. This is required for these clusters to have evaporated, being completely disrupted either by the energy injections of the first supernovae,⁹ or by tidal effects. In that case, star formation triggered by the wind/SN shocks from evolving massive stars might have been quenched, rendering impossible the birth of field stars with processed material.

Another possibility, also related to the high stellar density in GCs, could be that such an environment favors higher rotational velocities than less dense environments. It is however not obvious that denser environments would favor high rotational velocities, the stellar encounters being able of both spinning up the stars or slowing them down. The only thing we can say at

the moment is that some observations find higher rotational velocities in clusters than in the field: Huang & Gies (2006) determined the projected rotational velocities of 496 OB stars in clusters within the approximate age range 6-73 Myr. They found that there are fewer slow rotators among the cluster B-type stars relative to nearby B stars in the field. Strom et al. (2005) also found that stars in h and χ Persei tend to rotate faster than the field stars counterparts. A similar conclusion has been reached by Dufton et al. (2006) on the basis of the rotational velocities of stars in the two clusters NGC 3293 and NGC 4755. Of course it is difficult at the present time to draw firm conclusions about the origin of this difference. Let us just note that these observations may support the view according to which stars born in dense environments may have faster rotational velocities than stars born in loose aggregates.

An alternative to this view is to consider that all the field stars were born in the progenitors of the present day globular clusters. Let us recall that field halo stars contain at least hundred times the mass in globular clusters (Woltjer 1975). The above scenario would therefore imply a very efficient mechanism that would remove 99% of stars initially formed in the progenitor of the present day GC. Moreover, this mechanism should either be more rapid than the enrichment of the interstellar medium by massive stars, or should only remove stars with no chemical inhomogeneities. While it appears difficult to favor such a view, it would have the advantage of making the stars presenting inhomogeneities a very small subset of the whole stellar population in a given cluster and thus alleviate the need of a very flat IMF (PC06).¹⁰

8. Conclusion

The two main reasons why massive stars have been discarded in the past in the context of the GC self-enrichment scenario are related to the fact that these objects are expected to produce iron and to have fast winds.

In the present paper, we propose the Wind of Fast Rotating Massive Star scenario in order to explain the chemical inhomogeneities observed in GC stars. The key point of this scenario is the **fast rotation of massive stars**. Each one of these two characteristics is important:

- **Fast rotation** is needed to remove material from the stellar surface and inject it with a low velocity in the interstellar medium. It triggers internal mixing which brings to the surface material processed in the core. This enables a star to eject material with chemical compositions similar to that observed at the surface of GC stars.
- **Massive stars** have short lifetimes and can release H-synthesized material while low-mass stars are still forming in the nascent globular cluster. They can, through the wind and SN shocks or through the ionization front they produce, trigger star formation in their vicinity, being thus able to be at the same time the cause of new star formation and the provider of at least part of the material from which the stars form. Moreover, it appears that rotating massive stars can lose low-speed material only enriched in H-burning products. Low- and intermediate-mass stars would not be able to do that, either because they are less efficiently mixed by rotation and/or they have more difficulty to reach the break-up

⁸ At this stage, the critical velocity is lowered with respect to its classical expression (see Maeder & Meynet 2000).

⁹ It is interesting to note that the gravitational energy of a globular cluster is of the order of 10^{51} erg i.e. of the same order of magnitude as the kinetic energy emitted by a core collapse supernova explosion.

¹⁰ Since massive stars are preferentially located in the central parts of a young cluster, they may have polluted mainly the central regions. The outer part of the GC progenitors would at least for a while be composed of non polluted stars which may have been stripped off by tidal effects.

limit and of course the Ω -Limit than the massive stars during the main sequence. In addition their central temperature is too low to efficiently activate NeNa and MgAl chains during the MS. Besides they require a more top-heavy IMF than massive stars as explained by PC06.

Globular clusters may be suitable environments to form fast rotating massive stars in the proper range of metallicity. It is interesting to recall that the WFRMS scenario for explaining the GC abundance anomalies is only one consequence of fast rotation of massive stars. This kind of stars might be also interesting for understanding other features as the origin of the carbon-rich ultra metal-poor stars, the high N/O ratio observed in halo stars, and the high helium abundance of a part of stars in ω Cen (Maeder & Meynet 2006). The anticorrelations observed in GC might thus be an additional observed consequences of the chemical enrichment expected from fast rotating massive stars.

Acknowledgements.

References

- Alexander, D. R. & Ferguson, J. W. 1994, *ApJ*, 437, 879
 Angulo, C., Arnould, M., Rayet, M., et al. 1999, *Nuclear Physics A*, 656, 3
 Arnould, M., Goriely, S., & Jorissen, A. 1999, *A&A*, 347, 572
 Brown, J. A. & Wallerstein, G. 1993, *AJ*, 106, 133
 Carretta, E., Bragaglia, A., & Cacciari, C. 2004, *ApJ*, 610, L25
 Carretta, E., Bragaglia, A., Cacciari, C., & Rossetti, E. 2003, *A&A*, 410, 143
 Carretta, E., Gratton, R. G., Lucatello, S., Bragaglia, A., & Bonifacio, P. 2005, *A&A*, 433, 597
 Chaboyer, B. & Zahn, J.-P. 1992, *A&A*, 253, 173
 Charbonnel, C. 2005, in *IAU Symposium*, ed. V. Hill, P. François, & F. Primas, 347–356
 Coc, A., Vangioni-Flam, E., Descouvemont, P., Adahchour, A., & Angulo, C. 2004, *ApJ*, 600, 544
 Cohen, J. G., Briley, M. M., & Stetson, P. B. 2002, *AJ*, 123, 2525
 Cottrell, P. L. & Da Costa, G. S. 1981, *ApJ*, 245, L79
 de Jager, C., Nieuwenhuijzen, H., & van der Hucht, K. A. 1988, *A&AS*, 72, 259
 Denissenkov, P. A. & Herwig, F. 2003, *ApJ*, 590, L99
 Dickens, R. J., Croke, B. F. W., Cannon, R. D., & Bell, R. A. 1991, *Nature*, 351, 212
 Dufton, P. L., Ryans, R. S. I., Simón-Díaz, S., Trundle, C., & Lennon, D. J. 2006, *A&A*, 451, 603
 Fenner, Y., Campbell, S., Karakas, A. I., Lattanzio, J. C., & Gibson, B. K. 2004, *MNRAS*, 353, 789
 Freeman, K. C. & Norris, J. 1981, *ARA&A*, 19, 319
 Freyer, T., Hensler, G., & Yorke, H. W. 2003, *ApJ*, 594, 888
 Garcia-Segura, G., Langer, N., & Mac Low, M.-M. 1996, *A&A*, 316, 133
 Gnedin, O. Y., Zhao, H., Pringle, J. E., et al. 2002, *ApJ*, 568, L23
 Gratton, R., Sneden, C., & Carretta, E. 2004, *ARA&A*, 42, 385
 Gratton, R. G., Bonifacio, P., Bragaglia, A., et al. 2001, *A&A*, 369, 87
 Gratton, R. G., Sneden, C., Carretta, E., & Bragaglia, A. 2000, *A&A*, 354, 169
 Grundahl, F., Briley, M., Nissen, P. E., & Feltzing, S. 2002, *A&A*, 385, L14
 Hale, S. E., Champagne, A. E., Iliadis, C., et al. 2002, *Phys. Rev. C*, 65, 015801
 Hale, S. E., Champagne, A. E., Iliadis, C., et al. 2004, *Phys. Rev. C*, 70, 045802
 Harbeck, D., Smith, G. H., & Grebel, E. K. 2003, *AJ*, 125, 197
 Heger, A. & Langer, N. 2000, *ApJ*, 544, 1016
 Herwig, F. 2004a, *ApJ*, 605, 425
 Herwig, F. 2004b, *ApJS*, 155, 651
 Huang, W. & Gies, D. R. 2006, *ApJ*, 648, 580
 Iglesias, C. A. & Rogers, F. J. 1996, *ApJ*, 464, 943
 Iliadis, C., D’Auria, J. M., Starrfield, S., Thompson, W. J., & Wiescher, M. 2001, *ApJS*, 134, 151
 Ivans, I. I., Sneden, C., Kraft, R. P., et al. 1999, *AJ*, 118, 1273
 James, G., François, P., Bonifacio, P., et al. 2004a, *A&A*, 414, 1071
 James, G., François, P., Bonifacio, P., et al. 2004b, *A&A*, 427, 825
 Karakas, A. I. & Lattanzio, J. C. 2003, *Publications of the Astronomical Society of Australia*, 20, 279
 Kraft, R. P. 1994, *PASP*, 106, 553
 Kraft, R. P., Sneden, C., Langer, G. E., & Prosser, C. F. 1992, *AJ*, 104, 645
 Kudritzki, R.-P. & Puls, J. 2000, *ARA&A*, 38, 613
 Lamers, H. J. G. L. M., Snow, T. P., & Lindholm, D. M. 1995, *ApJ*, 455, 269
 Langer, N. 1998, *A&A*, 329, 551
 Maeda, K. & Nomoto, K. 2003, *ApJ*, 598, 1163
 Maeder, A. 1999, *A&A*, 347, 185
 Maeder, A. & Meynet, G. 2000, *A&A*, 361, 159
 Maeder, A. & Meynet, G. 2001, *A&A*, 373, 555
 Maeder, A. & Meynet, G. 2006, *A&A*, 448, L37
 Maeder, A. & Zahn, J.-P. 1998, *A&A*, 334, 1000
 Meynet, G., Ekström, S., Maeder, A., & Barblan, F. 2006, *ArXiv Astrophysics e-prints*
 Meynet, G. & Maeder, A. 1997, *A&A*, 321, 465
 Meynet, G. & Maeder, A. 2000, *A&A*, 361, 101
 Meynet, G. & Maeder, A. 2002, *A&A*, 390, 561
 Nugis, T. & Lamers, H. J. G. L. M. 2000, *A&A*, 360, 227
 Pasquini, L., Bonifacio, P., Molaro, P., et al. 2005, *A&A*, 441, 549
 Porter, J. M. & Rivinius, T. 2003, *PASP*, 115, 1153
 Powell, D. C., Iliadis, C., Champagne, A. E., et al. 1999, *Nucl. Phys. A*, 660, 349
 Prantzos, N. & Charbonnel, C. 2006, *A&A*, 458, 135
 Ramírez, S. V. & Cohen, J. G. 2002, *AJ*, 123, 3277
 Ramírez, S. V. & Cohen, J. G. 2003, *AJ*, 125, 224
 Rivinius, T. 2005, in *ASP Conf. Ser. 337: The Nature and Evolution of Disks Around Hot Stars*, ed. R. Ignace & K. G. Gayley, 178–+
 Sackmann, I.-J. & Anand, S. P. S. 1970, *ApJ*, 162, 105
 Salaris, M., Weiss, A., Ferguson, J. W., & Fusilier, D. J. 2006, *ArXiv Astrophysics e-prints*
 Shetrone, M. D. 1996, *AJ*, 112, 2639
 Smith, G. H. 1987, *PASP*, 99, 67
 Smith, G. H. 2006, *PASP*, in press
 Sneden, C. 2005, in *IAU Symposium*, ed. V. Hill, P. François, & F. Primas, 337–344
 Sobeck, J. S., Ivans, I. I., Simmerer, J. A., et al. 2006, *AJ*, 131, 2949
 Strom, S. E., Wolff, S. C., & Dror, D. H. A. 2005, *AJ*, 129, 809
 Talon, S. 2004, in *IAU Symposium*, ed. A. Maeder & P. Eenens, 336–+
 Townsend, R. H. D., Owocki, S. P., & Howarth, I. D. 2004, *MNRAS*, 350, 189
 Ventura, P. & D’Antona, F. 2005a, *A&A*, 431, 279
 Ventura, P. & D’Antona, F. 2005b, *A&A*, 439, 1075
 Ventura, P. & D’Antona, F. 2005c, *ApJ*, 635, L149
 Ventura, P. & D’Antona, F. 2006, *A&A*, 457, 995
 Ventura, P., D’Antona, F., & Mazzitelli, I. 2002, *A&A*, 393, 215
 Ventura, P., D’Antona, F., Mazzitelli, I., & Gratton, R. 2001, *ApJ*, 550, L65
 Wallerstein, G., Myckky-Leep, E., & Oke, J. B. 1987, *AJ*, 94, 523
 Woltjer, L. 1975, *A&A*, 42, 109
 Yong, D., Aoki, W., & Lambert, D. L. 2006, *ApJ*, 638, 1018
 Yong, D., Grundahl, F., Lambert, D. L., Nissen, P. E., & Shetrone, M. D. 2003, *A&A*, 402, 985
 Yong, D., Grundahl, F., Nissen, P. E., Jensen, H. R., & Lambert, D. L. 2005, *A&A*, 438, 875
 Zahn, J.-P. 1992, *A&A*, 265, 115